RICE UNIVERSITY

Design of vibration inspired bi-orthogonal wavelets for signal analysis

by

Quan Phan

A THESIS SUBMITTED
IN PARTIAL FULFILLMENT OF THE
REQUIREMENTS FOR THE DEGREE

Master of Science

APPROVED, THESIS COMMITTEE

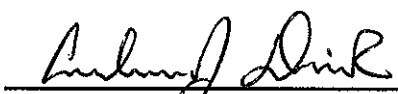

Andrew J. Dick, Chair
Assistant professor, Mechanical Engineering and Material Science Department

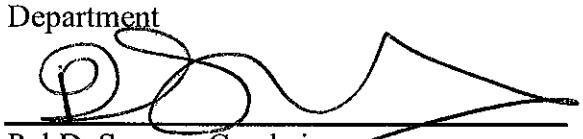

Pol D. Spanos, Co-chair
Lewis B. Ryon Professor of Mechanical Engineering and Materials Science, Mechanical Engineering and Material Science Department

Ilinca Stanciulescu
Assistant Professor, Civil and Environmental Engineering Department

HOUSTON, TEXAS
April 2012

ABSTRACT

Design of vibration inspired bi-orthogonal wavelets for signal analysis

by

Quan Phan

In this thesis, a method to calculate scaling function coefficients for a new bi-orthogonal wavelet family derived directly from an impulse response waveform is presented. In literature, the Daubechies wavelets (DB wavelet) and the Morlet wavelet are the most commonly used wavelets for the dyadic wavelet transform (DWT) and the continuous wavelet transform (CWT), respectively. For a specific vibration signal processing application, a wavelet that is similar or is derived directly from the signal being studied proves to be superior to the commonly used wavelet. To assure a wavelet has a direct relationship to the signal being studied, a new formula is proposed to calculate coefficients which capture the characteristics of an impulse response waveform. The calculated coefficients are then used to develop a new bi-orthogonal wavelet family. The new bi-orthogonal wavelet family is expected to provide better system characteristic enhancements to identify minor changes to the characteristics of the system being studied.

Acknowledgments

I would like to express my thankfulness to my direct advisor Dr. Andrew Dick for giving me the chance to work under his guidance. Thank you for your constant support and guidance. Without you, I don't know about wavelets. I would like to express my gratitude to Dr. Pol Spanos for his generosity. Thank you for sharing your knowledge, experience and expertise thought in my subject. I would also like to give my thankfulness to Dr. Ilinca Stanciulescu for agreeing to serve on my committee.

The financial support from the Vietnam International Education Development fellowship for the first two years and research assistantships from the Rice University in my third year is gratefully acknowledged.

Finally, to my family, without them I cannot finalize this thesis work. Thanks for loving me.

Contents

List of Figures

List of Tables

Nomenclature

BDWT	Bi-orthogonal dyadic wavelet transform
CWT	Continuous wavelet transform
DB1-10	Daubechies wavelet 1-10
DWT	Dyadic wavelet transforms
FIR	Finite impulse response
ODWT	Orthogonal dyadic wavelet transform
SDOF	Single degree of freedom
SNR	Signal to noise ratio
STFT	Short time Fourier transform

Chapter 1

Introduction

1.1. Literature survey and motivations

Since the 1990's, the wavelet transform has been widely recognized as a tool to analyze transient behaviors in signals (J. Ling, 2000) (Z.K. Peng, 2004) (P.D. Spanos, 2005) (Z. Kunpeng, 2009) (J. Rafiee, 2010).

The first work on wavelets was attributed to Morlet (P. Goupillaud, 1984) who derived the formulation of the wavelet transform to analyze seismic signals. Then, the connection between the wavelet transform and the multi-resolution analysis was identified. For a useful wavelet, Daubechies proposed a discrete, maximally flat, compactly supported, orthogonal wavelet family known as the Daubechies wavelets (Daubechies, 1988) (Daubechies, 1992). This wavelet family became a popular wavelet for signal processing applications (B. Zeldin, 1996). For wavelet coefficient calculations, a fast wavelet algorithm that is based on the

pyramid structural of filter banks was proposed by Mallat (Mallat, 1989). This fast wavelet algorithm could reach to O(N) computational complexity.

After that, Cohen, Daubechies and Feauveau relaxed the orthogonality condition in the dyadic orthogonal wavelet and proposed the Cohen Daubechies Feauveau bi-orthogonal wavelet family which was regarded as the first bi-orthogonal wavelet family (A. Cohen, 1992). The bi-orthogonal wavelet may have symmetric characteristics that are unexpected in the orthogonal wavelets. Currently, the Bpline bi-orthogonal wavelet family is the popular bi-orthogonal wavelets in literature because of its maximally flat filter characteristic (P.D. Spanos, 2001).

The popular wavelets were mostly derived from mathematical properties such as ortho-normality, symmetry and the maximally flat condition and these wavelets do not have relationship to a signal of interest. This fact limits the wavelet transform performance to enhance special features of the signal. There are two approaches to find the best wavelet for a signal being studied: (1) to find the best wavelet to represent the signal from available wavelet options and (2) to create a new wavelet that has a direct relationship to the signal.

The first approach was addressed by Tewfix, Shiha and Jorgensen (A.H. Tewfix, 1992) to find an optimal orthogonal wavelet to represent a signal of interest. An optimal orthogonal wavelet for the signal was identified by minimizing an

energy norm error function between the signal and its expansion on a wavelet subspace.

Next, Schukin, Zamaraev and Schukin addressed this problem for the impulse analysis of the vibration signals (E.L. Schukin, 2004). They assessed the performance of ten popular wavelets to identify impulse characteristics of the vibration signals. Their study showed that the impulse response wavelet was the best wavelet for this application.

In 2005, Fernando and Raghuveer applied the wavelet transform to identify faults in a mechanical system during impulse tests (S.N. Fernando, 2006). In their work, the Daubechies 2 (DB2) wavelet successfully located changes in the wave shape at faulty points. The study went further by suggesting that a better performance of the fault identification scheme could be achieved by an optimal wavelet.

For identifying faults in a bearing system under impulse excitations, Juncheng, Dejie and Yu proposed two methods that used wavelets to enhance fault features in the signal of interest (C. Juncheng, 2007). In their study, the continuous wavelet transform (CWT) provides a better time-frequency resolution than the dyadic wavelet transform, and the magnitude of the CWT coefficients reflects the similarity between the signal being studied and the wavelet at each time-scale point. They proposed the scale wavelet power spectrum method (in the frequency domain) and time-wavelet energy spectrum autocorrelation analysis method (in the

time domain) to identify faults, fault locations and fault patterns on the rolling bearing. These methods are based on the idea that the faulty excitations (impulse excitations) have transient characteristic and excite even high frequency modes of the bearing system. The fault identification performance confirmed that the impulse response wavelet provided better fault enhancements than the popular Morlet wavelet.

Rafiee, Rafiee and Tse recognized that the higher orders Daubechies wavelets have strong differences in their shape. They used 324 wavelets to analyze vibration signals and identified the DB44 wavelet provides the best performance in an average sense to analyze the vibration signal due to being nearly symmetric and having similar property with the signal of interest. In addition, their study also pointed out that a proper process should be implemented to identify a suitable wavelet for each wavelet based signal processing procedure (J. Rafiee, 2010).

For the second approach, a good wavelet for an application is identified by directly designing a new wavelet from a signal of interest. In 2000, Chapa and Rao designed an ortho-normal wavelet that matched to a signal of interest by minimizing an energy error function in the frequency domain between the signal and the wavelet at an optimal scale (J.O. Chapa, 2000).

For a signal de-noising application, Shark and Yu constructed an optimal ortho-normal wavelet based on the genetic algorithm in a shift invariant property

sense (L.K. Shark, 2003). They proved that the constructed ortho-normal wavelet was better than the Daubechies wavelet in this application.

Then, Gupta, Joshi and Prasad designed a wavelet by projecting characteristics of a signal of interest on the scaling function coefficients (A. Gupta, 2005). In their study, a desired number of vanishing moments can be added into the new bi-orthogonal wavelet. This feature improves the performance of the new bi-orthogonal wavelet to localize the signal features.

For identifying wave dispersion characteristic, in 2008 Bussow addressed this problem to compensate the current limitations of the classical autocorrelation and spectral methods for this application. The performance of an existing identification scheme is improved by using a new wavelet that had dispersion characteristic which is similar to the waveform of interest (Bussow, 2008). The new wavelet could be used to capture both the distance between the source and the receiver of an impulse wave and the material properties with only one measurement. In addition, this new wavelet also had an ability to analyze two overlapping pulses together which was limited with the Morlet wavelet.

For a criterion to select a wavelet to analyze a vibration signal, a quantitative measure based on the energy to Shannon entropy ratio was proposed by Yan and Gao (R. Yan, 2009). By using the proposed criterion, the study showed that the complex Morlet wavelet provides the best performance for a bearing defect diagnosis. Then, they proposed a method to design a new discrete impulse wavelet

that matched the impulse responses of a rolling bearing (R. Yan, 2010). This method was based on a similarity in the form between the convolution integral in linear system theory and the dilation equation in wavelet theory. An optimal energy error function was derived to minimize the difference between the wavelet coefficients and the impulse response signal. Their results showed that the new bi-orthogonal wavelet performed better than the widely used DB wavelet in analyzing impulse responses of roller bearing.

Both of the approaches to find an optimal wavelet for a signal of interest confirmed that a proper process should be performed to identify a good wavelet for a signal of interest. The wavelet that was optimally selected or had a direct relationship to the signal of interest proved to have a better performance than the popular wavelets. Following the second approach, the thesis presents a new formula to calculate scaling function coefficients from an impulse response waveform. The derived scaling function coefficients are used as primal scaling function coefficients of a new bi-orthogonal wavelet family. The new wavelet family is expected to provide better system characteristic enhancements to identify slight changes in characteristics of mechanical systems.

1.2. Contribution of this thesis

In this thesis, a method to calculate scaling function coefficients that capture characteristics of a waveform is presented. Then, the calculated coefficients are used to design a new bi-orthogonal wavelet family. For a general signal, the

Daubechies wavelet (DB wavelet) and the Morlet wavelet are the most commonly used wavelet for the dyadic wavelet transform (DWT) and the continuous wavelet transform (CWT), respectively. For a particular signal, a wavelet that is similar to or is derived directly from the signal being studied proves to be superior to the commonly used wavelet. The new bi-orthogonal wavelet family is expected to provide better system characteristic enhancements to identify slight changes in characteristics of mechanical systems.

1.3. Background concepts

In this section, background concepts for the thesis materials are presented. First, a definition of system and signal are presented together with the study of the linear system responses under different types of excitations. Then, the definition of the convolution integral, base and frame, the Fourier transform and the wavelet transform are briefly reviewed.

1.3.1. System and signal

One definition of a system is stated: "A system is defined as a mathematical abstraction devised to serve as a model for physical phenomenon. It consists of an input function $p(t)$, an output function $u(t)$, and a cause effect relationship between them." (Weaver, 1993) A single input $p(t)$ and single output $u(t)$ system is illustrated in Figure 1.1.

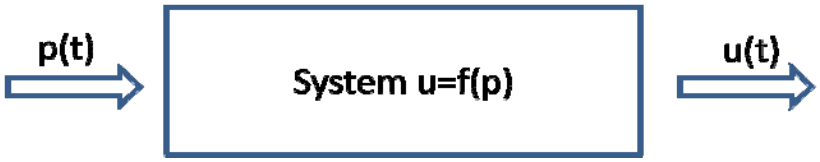

Figure 1.1 Relationship between a input and an output of a system

The simplest system is a linear time invariant single input single output system. This system satisfies the homogeneity and superposition properties that can be described by (1.1) and (1.2) below.

$$u(p_1)+u(p_2)=u(p_1+p_2), \tag{1.1}$$

$$ku(p_1)=u(kp_1). \tag{1.2}$$

These properties are also true for the general linear systems. For the case of a linear time invariant system, its behavior is described completely by an impulse response function. For example, a single degree of freedom (SDOF) spring mass damper system has an equation of motion in (1.3).

$$m\ddot{u}(t)+c\dot{u}(t)+ku(t)=p(t). \tag{1.3}$$

The system behavior is described by an impulse response function that has an analytical form given in (1.4).

$$h(t)=\frac{e^{-\xi\omega_n t}}{m\omega_d}\sin\omega_d t, \qquad \omega_d=\sqrt{1-\xi^2}\,\omega_n, \quad \omega_n=\sqrt{\frac{k}{m}}, \quad \xi=\frac{c}{2\sqrt{km}}, \tag{1.4}$$

where $h(t)$ is the impulse response, ω_d is the damped angular natural velocity, ω_n is the angular natural velocity and ξ is the damping ratio of the system. The system is linear therefore the output of the system is the summation of the response to each excitation. The relationship between the input and the output of the system can be represented by a Duhamel integral equation (convolution integral) in (1.5).

$$u(t) = \int_{-\infty}^{+\infty} p(\tau)h(t-\tau)d\tau. \tag{1.5}$$

If the excitation is an ideal impulse wave and the system is at rest, the system response is the impulse response function $h(t)$ defined in (1.4). The convolution integral can also be applied when the system is excited by a harmonics excitation such as $P(t) = P_0 \cos(\Omega t)$. The steady-state response of the system is also a harmonics function that has the same frequency but a different phase. A magnitude U and a phase difference α of the response are defined in (1.6).

$$U = \frac{U_0}{\left\{\left(1-\left(\frac{\Omega}{\omega_n}\right)^2\right)^2 + \left(2\xi\frac{\Omega}{\omega_n}\right)^2\right\}^{\frac{1}{2}}}, \quad \tan\alpha = \frac{2\xi\frac{\Omega}{\omega_n}}{1-\left(\frac{\Omega}{\omega_n}\right)^2}. \tag{1.6}$$

The magnitude of the system response is a frequency dependent function. The resonance behavior in the system occurs if the excitation frequency is close to a characteristic frequency of the system. There is no time information of the system response in this description. In the case of a linear time invariant system, the

system response at the harmonic excitation frequency is sufficient to describe the steady-state system behavior at the frequency of the excitation. If the system parameters are time dependent, the response of the harmonic excitation is the average information of the system response at the excitation frequency and is not sufficient to represent the system behavior.

For a third excitation type, the system is excited by a small wave that is defined by a sinusoid with a Gaussian envelope. The analytical form of the small wave is in (1.7).

$$p(t) = \cos(2\pi t)e^{\frac{-t^2}{2}}. \tag{1.7}$$

The system response has both the 'small wave' characteristics and the system impulse response characteristics. Also, the system response decays over time. If the small wave characteristics are similar to the system impulse response characteristics, the system response magnitude is larger. By applying a small wave excitation, the system configuration can be identified with both time and small wave characteristic information. A wavelet is a small wave in general. These three types of excitation demonstrate why the wavelet transform is more helpful in analyzing information of a transient signal than the Fourier transform. If the small wave has similar characteristics to the impulse response of the system, this property will enlarge the system characteristics onto the output of the system response.

1.3.2. Convolution integral

The convolution integral is an operator that is used to measure the similarity between two functions $f(t)$ and $g(t)$ that is defined in continuous form by (1.8) and in discrete form by (1.9).

$$h(t) = (f * g)(t) = \int_{-\infty}^{+\infty} f(\tau) g(t-\tau) d\tau, \tag{1.8}$$

$$(f * g)(n) = \sum_{m=-\infty}^{\infty} f(m) g(n-m). \tag{1.9}$$

One of the important features of the convolution integral is a simple relationship in the frequency domain. The convolution integral has the form in the time domain as defined in (1.8) which is equivalent to the form $H(\omega) = F\omega)G(\omega)$ in the frequency domain where $H(\omega)$, $F(\omega)$ and $G(\omega)$ are the frequency representation of $h(t)$, $f(t)$ and $g(t)$, respectively. The relationship is fundamental to linear discrete time invariant filter theory.

1.3.3. Bases and Frames

The measured signals are generally in the discrete time domain that can be represented effectively by (1.10) by using the Dirac's delta functions.

$$\sum_{i=-\infty}^{\infty} x(k)\delta_0(k) = x(0), \tag{1.10}$$

where the Dirac's delta functions have the form in (1.11).

$$\delta_j(k) := \begin{cases} 1 \text{ for } j = k \\ 0 \text{ for } j \neq k \end{cases}. \tag{1.11}$$

However, this representation only provides the time information of the signal but lacks the frequency information which is important to understand system behavior. Therefore, the signal in the time domain is transformed into the frequency domain by projecting the time domain signal onto the sinusoid base. This transformation is called the Fourier transform. The definition of a base is: "A base is a sequence of vectors υ_1, υ_2, … or functions v_1, v_2 … with property of unique representation" (G. Strang, T. Nguyen, 1996). The Dirac's delta functions are a base to represent the signal in the time domain and the sinusoid functions are a base to represent the signal in the frequency domain. The projection of a time sequence x to a sinusoid function y is defined by an inner product operator in a continuous form by (1.12).

$$< x, y >= \int_{-\infty}^{\infty} x^*(t) y(t) dt, \tag{1.12}$$

The function $x*(t)$ is the complex conjugate of $x(t)$. The norm that is defined in the Hilbert space L^2 has the form in (1.13).

$$\|x\| = \sqrt{< x, x >} = \sqrt{\sum_{i=-\infty}^{\infty} \left| x_i^{\,2} \right|}. \tag{1.13}$$

The Diract's delta function and the sinusoid function are ortho-normal bases in the time and frequency domains respectively. This characteristic permits a simple representation of a signal by a linear summation of the projected signal on each time step in the time domain and each frequency component basis φ_i in the frequency domain as shown in (1.14).

$$f(x) = \sum_{i \in J} < \varphi_i, x > \varphi_i. \tag{1.14}$$

A frame is defined if we have more than one representation of a function $f(x)$ on a set of basis. The wavelet transform is a new base that represents the signal in a wavelet domain. The wavelet basis is compactly supported in both time and frequency domain therefore the representation provides not only time information but also frequency information of the signal simultaneously. The representation of the signal on the wavelet domain is an alternate tool to enhance the signal characteristics especially for the transient or non-stationary signals that the Fourier transform cannot effectively represent.

1.3.4. The Fourier transform

Given a function $f(t)$, the Fourier transform of the function is defined by (1.15) below.

$$F(\omega) = \int_{-\infty}^{\infty} f(t) e^{-2\pi i \omega t} dt, \tag{1.15}$$

and its inverse pair is defined by (1.16).

$$f(t) = \int_{-\infty}^{\infty} F(\omega) e^{2\pi i \omega t} d\omega. \tag{1.16}$$

From the definition, the Fourier transform is a series of harmonic oscillations that cover the frequency domain and provides averaged frequency information of the signal in the whole time domain. In the real world, most systems are sensitive to excitations that are closed to resonance frequencies and the Fourier transform is a suitable tool to study time invariant signals. In 1966, Cooley and Tukey invented the Fast Fourier transform algorithm that reduced the calculation complexity of the discrete Fourier transform to NlogN (C.S. Burrus, 1997).

One improvement on the Fourier transform to localize its bases by a window function is the Short Time Fourier Transform (STFT). The transform localizes time information of the signal that is defined in (1.17).

$$STFT_f(\omega, \tau) = \int_{-\infty}^{\infty} e^{-j\omega t} g^*(t-\tau) f(t) dt, \tag{1.17}$$

where $e^{-j\omega t}$ is the basis function of the Fourier transform, $f(t)$ is the signal of interest and $g(t-\tau)$ is the time window function. However, the time support of the window function is constant. The STFT does not effectively analyze the low frequency content or the high frequency content of the signal of interest.

1.3.5. The wavelet transform

The Fourier transforms is problematic with non-stationary and transient signals. The issue was solved by defining a function that had the time window support length adaptively compress at the high frequencies and elongate at the low frequency content of the signal to achieve a maximum time-frequency resolution in the time-frequency plane. In 1984, Morlet formulated a new transform for seismic signal analysis by a function that adaptively represents information in the time-frequency plane (P. Goupillaud, 1984). His transform is then called the wavelet transform that has the basic formulation in (1.18).

$$W(a,b) = \frac{1}{\sqrt{a}} \int_{-\infty}^{\infty} f(t)\psi(\frac{t-b}{a})dt. \tag{1.18}$$

The mother wavelet function $\psi(t)$ can be understood as a small wave excitation of a signal of interest or system. The formula of the inverse version of the wavelet transform which is defined in a least square sense is represented in (1.19).

$$f(t) = \frac{1}{C_\psi} \int_{-\infty}^{\infty}\int_{-\infty}^{\infty} \frac{1}{a^2} W(a,b)\psi(\frac{t-b}{a})dadb. \tag{1.19}$$

Strictly speaking, the mother wavelet function must satisfy the admission condition which defined in the time domain by (1.20) and in the frequency domain by (1.21).

$$\int_{-\infty}^{\infty} \psi(t)dt = 0, \tag{1.20}$$

$$0 < C_{\psi} = \int_{-\infty}^{\infty} \frac{|\Psi(\omega)|^2}{|\omega|} d\omega < \infty, \tag{1.21}$$

where C_{ψ} is the admissibility constant and $\Psi(\omega)$ is the frequency representation of the wavelet respectively. Since discovered, the wavelet transform has been applied in many fields including physics, math, and engineering to study the transient behavior of signals (Z.K. Peng, 2004) (Z. Kunpeng, 2009).

1.4. Organization of this thesis

The thesis is organized in the following order. Chapter 2 presents the wavelet transform representation and its classifications. In chapter 3, a formula to calculate scaling function coefficients of a new bi-orthogonal wavelet is presented. Verification, analysis, and a method to qualitatively evaluate the accuracy of the formula to capture signal characteristics are also presented in this chapter. Conclusions and future work are then in the final chapter.

Chapter 2

Wavelet representation

2.1. Wavelets and the wavelet transform

The wavelet transform is defined by a convolution integral between a scaled and translated mother wavelet function $\psi\left(\frac{t-b}{a}\right)$ and a signal $f(t)$. The transform expands the signal $f(t)$ in time domain into a time and scale representation $W(a,b)$. The definition of the wavelet transform is defined in (2.1).

$$W(a,b) = \frac{1}{\sqrt{a}} \int_{-\infty}^{\infty} f(t)\psi(\frac{t-b}{a})dt, \qquad (2.1)$$

where $W(a,b)$ is a wavelet coefficient at a scale a and translation b. The mother wavelet function works as a small wave that translates and scales to measure the similarity between the mother function and a signal at each scale a and translation b on the time scale representation. In order to guarantee for a perfect

reconstruction, the mother wavelet function must satisfy the finite energy condition. These conditions can be represented under the admission conditions for a mother wavelet function in the time domain by (2.2) and in the frequency domain by (2.3).

$$\int_{-\infty}^{\infty} \psi(t)dt = 0, \tag{2.2}$$

$$C_{\psi} = \int_{-\infty}^{\infty} \frac{|\Psi(\omega)|^2}{|\omega|} d\omega < \infty. \tag{2.3}$$

The conditions in (2.3) and (2.4) allow for the variety of wavelet bases in the literature. Then, the original function can be recovered from the wavelet transform coefficients by its inverse transform in (2.4).

$$f(t) = \frac{1}{C_{\psi}} \int_{-\infty}^{\infty}\int_{-\infty}^{\infty} \frac{1}{a^2} W(a,b)\psi(\frac{t-b}{a})dadb. \tag{2.4}$$

In general, the wavelet transform can be applied as the continuous wavelet transform (CWT) or the dyadic wavelets transform (DWT). The CWT translates and scales the mother wavelet function smoothly on a time scale representation but the DWT is based on the multi-resolution analysis theory. The mother wavelet function of the CWT has an analytical form on the contrary to the DWT that are defined by a low pass and high pass filter pair and in general do not have an analytical form. The filter pair of the DWT serves as the translation bases on each scaling function subspace and wavelet subspace of a multi-resolution decomposition on a $L^2(R)$ signal space.

Criteria to select a mother wavelet function for the CWT and the DWT are also largely different. For the DWT, the most popular wavelet family is the Daubechies wavelets due to its ortho-normal and optimal property in the number of vanishing moment in a provided compactly supported time space (Daubechies, 1988) (Daubechies, 1992). However, a leakage behavior usually appears between each scale of the DWT. For the Daubechies wavelet, leakage behavior of the Daubechies wavelet expansion is reduced when the length of the Daubechies wavelet filter increases (S. Mikami, 2011).

A mother wavelet for the CWT is selected based on the similarity between the mother wavelet and the signal of interest, phase map and time-frequency resolution (Staszewski, 1998) (D. Boulahbal, 1999) (X. Jiang, 2011). For the time-frequency resolution criterion, the Morlet wavelet is preferred due to its optimal property in this feature (P. Goupillaud, 1984). In general, a signal processing scheme performs better if a wavelet and a signal of interest have a direct relationship or are similar for both the CWT and the DWT (L.K. Shark, 2003) (C. Juncheng, 2007) (Bussow, 2008).

In summary, the wavelet transform provides different ways to represent a signal on the time-frequency plane. A wavelet should be selected based on special features of a particular signal processing application. The material of this chapter is organized in the following order. First, the dyadic orthogonal wavelet and its transform are reviewed through a multi-resolution analysis of a signal $f(t) \in L^2(R)$. After that, an expansion of the orthogonal dyadic wavelet transform (ODWT), the bi-

orthogonal dyadic wavelet transform (BDWT), is presented. The bi-orthogonal wavelets relax constraints of the orthogonal wavelets and provide more space in designing new wavelets. The orthogonal dyadic and the bi-orthogonal dyadic wavelets are presented in detail in the next section.

2.2. Dyadic wavelets and the dyadic wavelet transform

The dyadic wavelet transform (DWT) is defined by a pair of finite impulse response (FIR) filters and decomposes a $L^2(R)$ signal into a number of wavelet subspaces at different scales by a multi-resolution analysis. Each scaling function and wavelet subspace is a translation span of compactly supported scaling function and wavelet coefficients at a scale. This representation permits for the wavelet transform to localize the time information of a signal at each scale. For the wavelet transform coefficient calculation, Mallat proposed a fast wavelet transform algorithm that reduced the calculation complexity of the wavelet transform to O(N) (Mallat, 1989).

2.2.1. Multi resolution analysis, ortho-normal wavelets and the ortho-normal dyadic wavelet transform

The definition of a multi resolution analysis of a function $f(t) \in L^2(R)$ can be stated as follows: "A multi-resolution analysis of a function $f(t) \in L^2(R)$ is to iteratively decompose the function into a number of subspaces at different scales."

(G. Strang, T. Nguyen, 1996). The subspace V_j satisfies four conditions that are listed below:

- $V_j \subset V_{j+1}$ and $\bigcap_{j=-\infty}^{\infty} V_j = \{0\}$ and $\bigcup_{j=-\infty}^{\infty} V_j = L^2$ for the completion.

- Scale invariance: if $f(t) \in V_j$ then $f(2t) \in V_{j+1}$.

- Shift invariance: if $f(t) \in V_0$ then $f(t-k) \in V_0$.

- Shift invariant basis: V_0 has an ortho-normal basis $\{\phi(t-k)\}$ or a Riesz basis $\{\phi'(t-k)\}$, $k \in Z$.

A multi-resolution analysis in the wavelet domain is based on the dilation equation in (2.5) that relates the scaling function between two consecutive scales.

$$\varphi(t) = \sum_n h_0(n)\sqrt{2}\varphi(2t-n), \qquad n \in Z, \tag{2.5}$$

where $h_0(n)$ is the n^{th} scaling function coefficient and $\varphi(t)$ is the scaling function. The scaling function waveform is generated by iterating the dilation equation to convergence and its characteristics depend on the scaling function coefficients. Then, for the DWT, its scaling function does not generally have an analytical form. The function $\varphi(t)$ and its translated version $\varphi_k(t) = \varphi(t-k)$ define a base in $L^2(R)$ that span a scaling function subspace $V_0 = \overline{Span\{\varphi_k(t)\}}$ at a scale 0. If the scaling

function forms an orthogonal translation in V_0, the function $f_0(t)$ that belongs to the subspace V_0 can be represented by (2.6).

$$f_0(t) = \sum_k a_k \varphi_k(t), \qquad k \in Z, \tag{2.6}$$

where a_k is the projection coefficients of the function $f_0(t)$ to the scaling function $\varphi_k(t)$. Define a subspace $V_1 = \overline{Span\{\varphi_k(2t)\}}$ is the span of the function $\varphi(2t)$ and its translated version $\varphi_k(2t) = \varphi(2t-k)$. From the dilation equation, the expansion of function $f_0(t)$ on the V_0 subspace can also be represented by the span of the function $\varphi(2t)$ and its translated version $\varphi_k(2t) = \varphi(2t-k)$ in (2.7).

$$f_0(t) = \sum_k a_k \varphi_k(t) = \sum_k a_k \sum_n h_0(n)\sqrt{2}\varphi(2(t-k)-n), \qquad k, n \in Z. \tag{2.7}$$

Then, the expansion of function $f_0(t)$ also belongs to the subspace V_1. Recursively, a function $f_j(t)$ that belongs to the subspace $V_j = \overline{Span\{\varphi_k(2^j t)\}}$ is the span of the function $\varphi(2^j t)$ and its translated version $\varphi_k(2^j t) = \varphi(2^j t - k)$ and the subspace V_j covers the subspaces $V_0, V_1, \ldots, V_{j-1}$. In addition, the translation n step of the function $f_0(t)$ is $f_0(t+n) = \sum_k a_k \varphi_k(t+n)$ and also belongs to the subspace V_0.

From the analysis above, the scale invariance and shift invariance properties of the multi resolution analysis for the wavelet domain are satisfied with the dilation equation in (2.5).

For a completeness of the multi-resolution analysis on the wavelet domain, the scaling function and the scaling function coefficients must satisfy admission conditions. These conditions for the scaling function are defined in the time domain by (2.8) and in the frequency domain by (2.9).

$$\int_{-\infty}^{\infty} \varphi(t)dt = 1, \tag{2.8}$$

$$\Phi(\pi) = 0, \tag{2.9}$$

These conditions are equivalent to the conditions of the scaling function coefficients in the time domain by (2.10) and in the frequency domain by (2.11).

$$\sum_n h_0(n) = \sqrt{2}, \text{ and } \sum_n h_0(2n) = \sum_n h_0(2n+1) = \frac{1}{\sqrt{2}}, \qquad n \in Z \tag{2.10}$$

$$H_0(0) = \sqrt{2}, \tag{2.11}$$

with $H_0(0)$ is the frequency representation of the scaling function coefficients at zero frequency. From the above analysis, the scaling function subspace at the next level covers the information of the scaling function subspace at the previous level. The subspace W_0 which is called the wavelet subspace is defined as a span of differences (detail information) between the scaling function subspace V_0 and scaling function subspace V_1. If the scaling function subspaces and the wavelet subspace are orthogonal for the orthogonal dyadic wavelet transform (ODWT), those relationships can be represented in (2.12).

$$V_1 = V_0 \oplus W_0, \tag{2.12}$$

with $\oplus$ is the direct sum operator between two orthogonal subspaces. The wavelet subspace W_0 belongs to the scaling function subspace V_1. As a result, W_0 bases are generated by a linear summation of the subspace V_1 bases in (2.13).

$$\psi(t) = \sum_n h_1(n)\sqrt{2}\varphi(2t-n). \qquad n \in Z \tag{2.13}$$

The function $\psi(t)$ is called the wavelet function and $h_1(n)$ is called the wavelet coefficients. Those functions serve as translation bases for the wavelet subspace W_0. Therefore a function $f_1(t)$ that belongs to the wavelet subspace W_0 can be represented by $\psi(t)$ and its translation version $\psi_k = \psi(t-k)$. The two scale relation of the scaling function and its corresponding wavelet function are presented in (2.5) and (2.13).

The admission conditions for the wavelet function are defined by (2.14) and for its coefficients in the time domain by (2.15) and in the frequency domain by (2.16), respectively.

$$\int_{-\infty}^{\infty} \psi(t)dt = 0. \tag{2.14}$$

$$\sum_n h_1(n) = 0, \tag{2.15}$$

$$H_1(0) = 0. \tag{2.16}$$

By iterating (2.12), the scaling function subspace V_2 that covers the subspace V_1 and V_0 can be represented in (2.17).

$$V_2 = V_0 \oplus W_0 \oplus W_1. \tag{2.17}$$

For a complete expansion of the scaling function on the $L^2(R)$ signal space, the decomposition of a signal $f(t) \in L^2(R)$ is the linear summation of an infinite number of orthogonal wavelet subspaces and the coarsest scaling function subspace V_0 as shown in (2.18)

$$V_0 \oplus W_0 \oplus W_1 \oplus W_2 \oplus W_3 \oplus ...W_N ...W_\infty = L^2(R). \tag{2.18}$$

The summation of the subspaces in the (2.18) is equivalent to the representation of an arbitrary signal $f(t) \in L^2(R)$ in (2.19).

$$f(t) = \sum_k < f, \phi_{0k} > \phi_{0k} + \sum_{j=0}^{\infty} \sum_k < f, \psi_{jk} > \psi_{jk}. \tag{2.19}$$

Beside the general conditions for the scaling function coefficients, the orthogonal relationship of the scaling function and its coefficients for an ODWT can be described by the inner product of the scaling function and its translation for the scaling function in (2.20) and for the scaling function coefficients in (2.21).

$$\int \varphi(t)\varphi(t-k)dt = \begin{cases} 1 & if\ k=0, \\ 0 & otherwise, \end{cases} \tag{2.20}$$

$$\sum_n h_0(n)h_0(n-2k) = \delta(k) = \begin{cases} 1 & if\ k=0, \\ 0 & otherwise. \end{cases} \tag{2.21}$$

For the ODWT, the wavelet function and its coefficients relate to its corresponding scaling function and scaling function coefficients in (2.22) and (2.23).

$$\int \varphi(t-n)\psi(t-m)dt = 0, \tag{2.22}$$

$$\sum_n h_0(n)h_1(n-2k) = 0. \tag{2.23}$$

Those relationships can be converted into a direct relation between wavelet coefficients and the scaling function coefficients in (2.24).

$$h_1(n) = (-1)^n h_0(N-n-1). \tag{2.24}$$

The variable *N* is the length of the scaling function coefficients. The scaling function coefficients and the wavelet coefficients of the ODWT satisfy the quadratic mirror filter condition which is defined in (2.25).

$$\left|H_0(\omega)\right|^2 + \left|H_1(\omega)\right|^2 = 2, \tag{2.25}$$

where $H_1(\omega)$ is the frequency representation of the wavelet coefficients. The scaling function and the wavelet coefficients of the ODWT at a scale j and a

translation k are calculated by projecting the function $f(t)$ to the scaling function and the wavelet function at a scale j and a translation k in (2.26) and (2.27).

$$c_k^j = \int_R f(t)\phi_{j,k}(t)dt, \tag{2.26}$$

$$d_k^j = \int_R f(t)\psi_{j,k}(t)dt, \tag{2.27}$$

where c_k^j is the scaling function coefficients of function $f(t)$ at the scale *j* and the translation *k*, d_k^j is the wavelet coefficients of function $f(t)$ at the scale *j* and the translation *k*. The coefficients also can be calculated directly from the approximation coefficients at the next scale by using (2.28) and (2.29).

$$c_k^j = \sum_n h_0(2k-n)c_{j+1}(n), \tag{2.28}$$

$$d_k^j = \sum_n h_1(2k-n)c_{j+1}(n). \tag{2.29}$$

From (2.28) and (2.29), the computational complexity of the wavelet expansion scheme reduces with the reduction of the length of the filter coefficients. The projection of the function $f(t)$ to the scaling function and wavelet subspaces V_j and W_j at a level j by the ODWT can be calculated directly in (2.30) and (2.31).

$$P_j(f(t)) = \sum_{k\in J} < f(t), \phi_{j,k} > \phi_{j,k} = \sum_{k\in J} c_k^j \phi_{j,k}, \tag{2.30}$$

$$Q_j(f(t)) = \sum_{k\in J} < f(t), \psi_{j,k} > \psi_{j,k} = \sum_{k\in J} c_k^j \psi_{j,k}, \tag{2.31}$$

Where $P_j(f(t))$ and $Q_j(f(t))$ are the projection of the function $f(t)$ onto the scaling function subspace V_j and the wavelet subspace W_j, respectively. The projection of the function $f(t)$ onto the scaling function subspace V_j can be iteratively calculated by the summation of the wavelet subspace and the scaling function subspace at the previous level in (2.32).

$$P_j(f(t)) = \sum_n P_{j-1}(f(t))h_0(2t-n) + \sum_n Q_{j-1}(f(t))h_1(2t-n). \tag{2.32}$$

The relationship in (2.32) is essential for the pyramid fast wavelet algorithm that was proposed by Mallat (Mallat, 1989) to calculate wavelet coefficients. In addition, the ODWT guarantees for the Parseval identity condition that can be described in (2.33).

$$\int |f(t)|^2 dt = \sum_{n=-\infty}^{\infty} |c_0(n)|^2 + \sum_{j=0}^{\infty}\sum_{m=-\infty}^{\infty} |d_j^k|^2. \tag{2.33}$$

From the analysis above, the DWT and its characteristics are described completely by a pair of scaling function and wavelet coefficients. For the ODWT, the approximation and the detail coefficients at a scale *j* and a translation *k* are calculated directly by projecting the function $f(t) \in L^2(R)$ onto the wavelet and scaling function at the scale j and the translation k. Also, the orthogonal characteristic both in translation and scaling function subspaces permits for the ODWT to guarantee the Parseval identity condition. The energy of a signal is conserved in the orthogonal wavelet domain. Two most desired characteristics for

the orthogonal wavelet and the scaling function coefficients are compactly supported and the number of vanishing moments. The first characteristic influences the computational efficiency of the wavelet transform and its ability to detect transient characteristics of a signal. The second characteristic gives the approximation property to the wavelet. This characteristic determines the order of the polynomial that the scaling function can exactly approximate (Daubechies, 1988) (Daubechies, 1992) (G. Strang, T. Nguyen, 1996).

The scaling function coefficients and the wavelet coefficients of the ODWT are under many constraints and only a very limited number of sets of coefficients satisfy those conditions. Some desired characteristics are lost such as linear phase. A more natural expansion of the ODWT is the bi-orthogonal dyadic wavelet transform (BDWT). The bi-orthogonal wavelet relaxes the orthogonal property of the ODWT and permits more space for wavelet design. The bi-orthogonal wavelets and its structure are presented in the next section.

2.2.2. Bi-orthogonal wavelets and the bi-orthogonal wavelet transform

The ODWT structure has been presented through a multi-resolution analysis on a $L^2(R)$ signal space in the previous section. The ODWT and its inversion use only a pair of scaling function and wavelet coefficients. It provides a simple decomposing scheme for a time-frequency analysis. Cohen, Daubechies and Feauveau generalized the orthogonal Daubechies wavelets and proposed a Cohen Daubechies Feauveau bi-orthogonal wavelet family (A. Cohen, 1992). For the bi-

orthogonal wavelet, a dual is introduced and the multi-resolution analysis for the bi-orthogonal wavelet case is also expanded to a dual multi-resolution analysis for a $f(t) \in L^2(R)$ signal. The definition of the bi-orthogonal wavelet and its transform are presented in this section.

The bi-orthogonal wavelet was developed by introducing a primal scaling function, a primal wavelet function, a dual scaling function and a dual wavelet function which can be described by the dilation equations and the wavelet equations in (2.34), (2.35), (2.36) and (2.37).

$$\phi(t) = \sum_k h_0(k)\phi(2t-k), \tag{2.34}$$

$$\tilde{\phi}(t) = \sum_k \tilde{h}_0(k)\tilde{\phi}(2t-k), \tag{2.35}$$

$$\psi(t) = \sum_k h_1(k)\psi(2t-k), \tag{2.36}$$

$$\tilde{\psi}(t) = \sum_k \tilde{h}_1(k)\tilde{\psi}(2t-k), \tag{2.37}$$

where $h_0(k)$ and $\tilde{h}_0(k)$ are the scaling function coefficients and the corresponding dual scaling function coefficients and $h_1(k)$ and $\tilde{h}_1(k)$ are the wavelet coefficients and the corresponding dual wavelet coefficients.

Similar to the ODWT, the primal scaling function and its wavelet function serve as a translation basis for a scaling function subspace V_0 and a wavelet

subspace W_0. Those representations also satisfy the multi-resolution analysis relation in (2.38) and (2.39) for both primal and its dual.

$$\varphi(t)=\sum_n h_0(n)\sqrt{2}\varphi(2t-n), \tag{2.38}$$

$$\tilde{\varphi}(t)=\sum_n \tilde{h}_0(n)\sqrt{2}\tilde{\varphi}(2t-n), \tag{2.39}$$

where $\tilde{V}_0$, $\tilde{W}_0$, and $\tilde{V}_1$ are the dual scaling function subspace, dual wavelet subspace and the successive dual scaling function subspace, respectively. Iterating the relationship in (2.38) and (2.39), a dual multi-resolution analysis of a $f(t)\in L^2(R)$ signal can be illustrated in (2.40) and (2.41).

$$\{0\}\ldots\subset V_{-1}\subset V_0\subset V_1\subset\ldots L^2(R), \tag{2.40}$$

$$\{0\}\ldots\subset \tilde{V}_{-1}\subset \tilde{V}_0\subset \tilde{V}_1\subset\ldots L^2(R). \tag{2.41}$$

Different from the ODWT, the bi-orthogonal wavelet filter coefficients are related to its dual scaling function coefficients to satisfy a perfect reconstruction condition. The relationship is given in (2.42).

$$h_1(n)=(-1)^n\tilde{h}_0(\tilde{N}-n-1) \quad \text{and} \quad \tilde{h}_1(n)=(-1)^n h_0(N-n-1), \tag{2.42}$$

where $\tilde{N}$ and N are the lengths of the primal scaling function and its corresponding dual scaling function coefficients, respectively. The bi-orthogonal scaling function coefficients and its corresponding dual scaling function coefficients

need to satisfy the scaling function coefficients conditions in (2.10) and (2.11). The primal scaling and wavelet function of the bi-orthogonal wavelet satisfy the orthogonality relation to its dual scaling and wavelet function. The bi-orthogonal relationship can be described in (2.43), (2.44), (2.45) and (2.46).

$$< \psi_{j,k}, \tilde{\psi}_{i,l} >= \delta_{ji}\delta_{kl}, \tag{2.43}$$

$$< \phi_{j,k}, \tilde{\psi}_{i,l} >= 0, \tag{2.44}$$

$$< \psi_{j,k}, \tilde{\phi}_{i,l} >= \delta_{ji}\delta_{kl}, \tag{2.45}$$

$$< \tilde{\phi}_{j,k}, \psi_{i,l} >= 0. \tag{2.46}$$

Those bi-orthogonal relationships can be represented by orthogonal relations between primal subspace and its dual subspace in (2.47).

$$W_j \perp \tilde{V}_j, \qquad \tilde{W}_j \perp V_j, \tag{2.47}$$

Those relationships are equivalent to the relationships between the primal scaling function coefficients and wavelet function coefficients to its corresponding dual scaling function coefficients and dual wavelet function coefficients in (2.48), (2.49), (2.50) and (2.51).

$$\sum_n h_0(n)\tilde{h}_0(n-2k) = \delta(k) = \begin{cases} 1 & \text{if } k = 0, \\ 0 & \text{otherwise,} \end{cases} \tag{2.48}$$

$$\sum_n h_1(n)\tilde{h}_0(n-2k) = 0, \tag{2.49}$$

$$\sum_n h_0(n)\tilde{h}_1(n-2k)=0, \tag{2.50}$$

$$\sum_n h_1(n)\tilde{h}_1(n-2k)=\delta(k)=\begin{cases}1 & \text{if } k=0,\\ 0 & \text{otherwise.}\end{cases} \tag{2.51}$$

In addition, the bi-orthogonal scaling and wavelet coefficient at a scale j and a translate k of a function $f(t)\in L^2(R)$ are calculated by the summation of the projection of $f(t)$ at a translate k to the scaling and wavelet on the whole subspace W_j and V_j in (2.52) and (2.53).

$$a_{jk}=\sum_{k\in J} f(t)\varphi_j(t-k), \tag{2.52}$$

$$d_{jk}=\sum_{k\in J} f(t)\psi_j(t-k). \tag{2.53}$$

Then, the projection of the function $f(t)$ to the bi-orthogonal scaling function and wavelet subspaces $\tilde{V}_j$ and $\tilde{W}_j$ at level j by the BDWT can be calculated in (2.54) and (2.55).

$$P_j(f(t)),=\sum_{k\in J}(\sum_{k\in J} f(t)\phi_j(t-k)_j)\phi_j(t-k), \tag{2.54}$$

$$Q_j(f(t))=\sum_{k\in J}(\sum_{k\in J} f(t)\psi_j(t-k)_j)\psi_j(t-k). \tag{2.55}$$

The function $f(t)\in L^2(R)$ can be recovered from its wavelet coefficients and dual wavelet in (2.56).

$$f(t) = \sum_{-\infty}^{\infty} \sum_{-\infty}^{\infty} d_{jk} \tilde{\psi}_{jk}(t). \tag{2.56}$$

2.3. Summary

The wavelet transform provides different ways to present a signal of interest. **The orthogonal wavelet is more popular than the bi-orthogonal wavelet because of its simpler representation and reconstruction the signal.** For designing a new wavelet, the bi-orthogonal wavelet requires fewer constraints than the orthogonal wavelet**. The materials in this chapter are used to derive a new bi-orthogonal wavelet that has characteristics of an impulse response waveform in its coefficients.**

Chapter 3

A Formula to calculate scaling function coefficients for a new bi-orthogonal wavelet family

The literature survey in chapter one identifies that a wavelet that has similar characteristics to the signal being studied performs better than the popular wavelet families. To study minor changes in the characteristics of a mechanical system under impulse excitations, a wavelet that has the same characteristics of the mechanical system is expected to perform better than popular wavelets such as Daubechies wavelets and Morlet wavelet. A formula derived from the dilation equation is proposed to calculate coefficients that capture the characteristics of an impulse response waveform input, referred to here after as “the Formula”. Then, a new bi-orthogonal wavelet family is designed directly from the calculated coefficients.

In this chapter, the derivation of the Formula is first presented. Then, the performance of the Formula is studied with the scaling functions of three Daubechies wavelets (DB2, DB3 and DB4). Next, analytical and experimental

impulse response waveforms are used to study the ability of the Formula to capture characteristics of the waveforms in a set of coefficients. In this step, to assure that the set of coefficients captures the characteristics of the waveform, a pre-process is implemented in order to identify a sufficient length of calculated coefficients.

The calculated coefficients are then used as an input for a bi-orthogonal wavelet design process. In this process, the calculated coefficients serve as the primal scaling function coefficients for a new bi-orthogonal wavelet. The new bi-orthogonal wavelet is then used to study characteristics of vibration signals together with the DB2 and the DB8 wavelet to evaluate its performance to identify minor changes in the system of being studied.

The process used to calculate coefficients by the proposed Formula, to study its performance with different waveforms and to design a new bi-orthogonal wavelet family from the calculated coefficients is presented in this chapter.

3.1. Derivation of the Formula

The dilation equation serves as the fundamental equation for the multi-resolution analysis of a signal $f(t) \in L^2(R)$. The equation relates the scaling function at one scale to the scaling function at the next scale. The dilation equation in the discrete form is restated in (3.1).

$$\varphi(t) = \sum_n h(n)\sqrt{2}\varphi(2t-n), \tag{3.1}$$

where $\varphi(t)$ is the scaling function at a scaling function subspace and $h(n)$ is the n^{th} scaling function coefficient. The right side of the dilation equation is equivalent to the convolution integral between the scaling function coefficients h and the scaling function at a previous scale or half-scale scaling function $\varphi(2t)$ in (3.2).

$$\varphi(t) = h * \varphi(2t), \tag{3.2}$$

where * denotes the convolution operation. The discrete version of the dilation equation can be represented in matrix form (Strang, 1989) as shown in (3.3).

$$[\varphi]_{1\times M} = [h]_{1\times N}[\varphi_{1/2}]_{N\times M}. \tag{3.3}$$

In matrix form, the scaling function coefficient $h(n)$ is a row vector of length N. The half-scale scaling function $\varphi_{1/2}$ is a vector of length $M/2$, which is then used to fill in a matrix with N rows and M columns. The half-scale scaling function is indexed in each successive row in order to place the vector along the diagonal of the matrix and the remainder of the matrix is filled with zeros. The resulting matrix is presented in (3.4).

$$[\varphi_{1/2}]_{N\times M} = \begin{bmatrix} [\varphi_{1/2}]_{1\times M/2} & \{0\} & \cdots & \{0\} \\ \{0\} & [\varphi_{1/2}]_{1\times M/2} & \cdots & \\ & & \ddots & \\ \{0\} & \{0\} & \cdots & [\varphi_{1/2}]_{1\times M/2} \end{bmatrix}. \tag{3.4}$$

The complete matrix form for the (3.3) is represented in (3.5).

$$[\varphi_{1/2}]_{1\times M} = \begin{bmatrix} h(1) & h(2) & \dots & h(N) \end{bmatrix} \begin{bmatrix} [\varphi_{1/2}]_{1\times M/2} & \{0\} & \dots & \{0\} \\ \{0\} & [\varphi_{1/2}]_{1\times M/2} & \dots & \\ & & \ddots & \\ \{0\} & \{0\} & \dots & [\varphi_{1/2}]_{1\times M/2} \end{bmatrix}. \quad (3.5)$$

The matrix equation (3.5) is then transposed to prepare to calculate coefficients $h(n)$, as shown in (3.6).

$$[\varphi]^T_{M\times 1} = [\varphi_{1/2}]^T_{M\times N}[h]^T_{N\times 1}. \quad (3.6)$$

Then, both sides of (3.6) are pre-multiplied by the inverse of matrix $[\varphi_{1/2}]^T_{M\times N}$. The coefficients $h(n)$ can be readily calculated from the waveform and its half scale using (3.7).

Since, the matrix $[\varphi_{1/2}]^T_{M\times N}$ is generally a non-square matrix, the standard matrix inverse procedure for a nonsingular square matrix cannot be applied. The Moore Penrose pseudo inverse based on a least square optimization is used to calculate the inverse of this non-square matrix $[\varphi_{1/2}]^T_{M\times N}$ (Penrose, 1955). A common implementation of the Moore Penrose pseudo inverse process is by the 'backsplash' operator in Matlab.

$$\{h\}^T_{N\times 1} = \left([\varphi_{1/2}]^T\right)^{-1}_{N\times M}\{\varphi\}^T_{M\times 1}. \quad (3.7)$$

The equation (3.7) provides the means to calculate a vector of coefficients representing an impulse response waveform. The process requires only two inputs: the discrete waveform and the length of the vector of calculated coefficients *N.* The process assumes that the non-square matrix $[\varphi_{1/2}]^T_{M\times N}$ is not ill-conditioned. The performance of the proposed Formula (3.7) is studied with different waveforms in the following sections.

3.2. Performance of the Formula with the Daubechies 2, 3, 4 scaling function waveforms

In this section, the performance of the Formula with the DB2, DB3 and DB4 scaling function waveforms is studied. Using common wavelet theory, an approximation of the Daubechies scaling function is calculated by successively iterating the dilation equation. The Daubechies 2 (DB2), Daubechies 3 (DB3) and Daubechies 4 (DB4) scaling function waveforms are generated by iterating the dilation equation from 4 to 14 times.

The procedure uses to convey the performance of the Formula with Daubechies scaling function waveforms is shown in Figure 3.1. Only two required inputs for the procedure are the Daubechies scaling function coefficients and the number of iterations. The performance of the proposed Formula is evaluated by comparing its calculated coefficients to the true values of the Daubechies scaling

function coefficients in a L^1 norm sense. In this study, the length of the vector of calculated coefficients N representing a waveform from their half-scale waveforms is known.

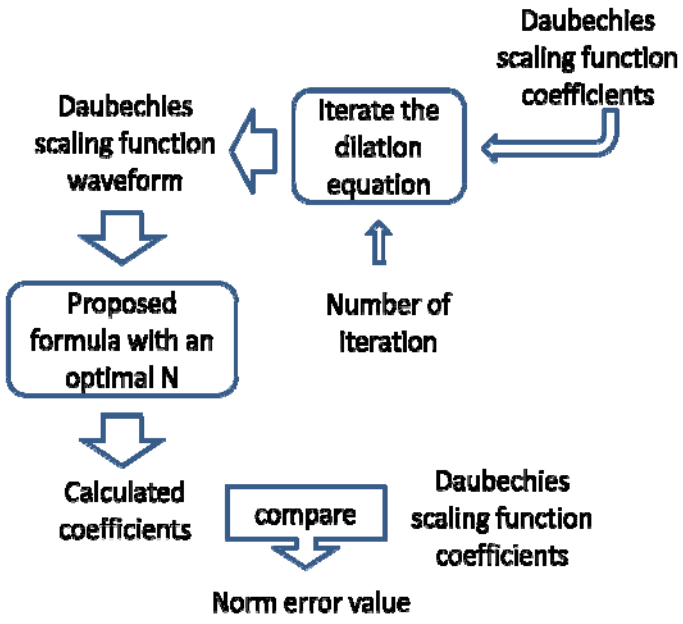

Figure 3.1 Procedure uses to convey the performance of the Formula with the Daubechies scaling function waveforms.

The norm error values associated with each iteration number and each corresponding Daubechies scaling function are plotted in Figure 3.2(A). The plots show that the error values are reduced by a factor of two with each increment in the number of iterations. This result is in agreement with general intuition that when the number of iterations is increased, a better approximation of the scaling function is achieved.

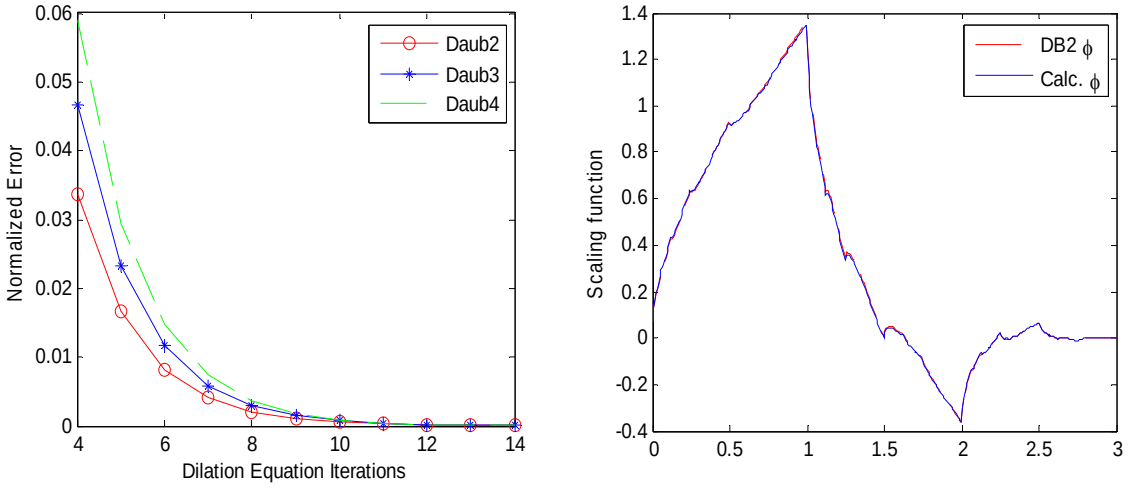

(A) (B)

Figure 3.2 (A) Plot of the error in the calculated scaling function coefficients versus the number of iterations of the dilation equation used to produce the scaling function of three different Daubechies wavelets. (B) Comparison of the scaling function obtained from the coefficient calculated by using the Formula to the Daubechies scaling function.

In addition, for the higher order Daubechies wavelet, additional iterations are required to archive the same level of calculation accuracy. The plot also indicates that the convergence rate of the iterative process to the true Daubechies scaling functions for the three DB wavelets are equal. A scaling function that is generated by the calculated coefficients at the same number of iterations is then compared to the original Daubechies scaling function. Illustrated in Figure 3.2(B), an excellent match between two functions is observed. Recalling that the Formula effectively calculates the coefficient set to represent the Daubechies scaling function from its half scale function. In the next section, the performance of the Formula is studied for both analytical responses and an experimental response.

3.3. Performance of the Formula applied to impulse response waveforms

In this section, analytical impulse response waveforms and an experimental waveform are used to study the performance of the proposed Formula. Although the waveforms are not identical to the scaling function, the form of the dilation equation still provides a good fit to calculate coefficients to represent the waveform by its half scale function. In this study, the sufficient length of the vector of calculated coefficients N is identified by an absolute error value between the original waveform and its representation by the half-scale waveform and the calculated coefficients. The performance of the Formula with analytical impulse response waveforms is presented first, then with an experimental waveform.

3.3.1. Analytical impulse response waveforms

In this study, the waveform is of the form of the impulse response of a linear and time invariant damped single degree of freedom oscillator. The form of the waveform is presented in (3.8).

$$f(t) = \frac{1}{m\omega_d} e^{-\zeta\omega_n t} \sin(\omega_d t). \tag{3.8}$$

The waveform characteristics depend on the natural frequency ω_n and the damping ratio ζ. The parameter m is the mass of the system and ω_d is the damped natural frequency calculated by $\omega_d = \omega_n\sqrt{1-\zeta^2}$. In this study, three different

analytical impulse response waveforms are constructed by using the three sets of system parameter values ω_n and ζ. The system parameter values are selected in order to study the performance of the Formula and do not consider physical meaning behind the analytical impulse response waveform. To allow for the impulse response waveform to sufficiently decay, the length of the waveform is selected to be an integer number of periods which is greater than five time constants.

Parameter set	Natural frequency	Damping ratio
1	π	0.3
2	π	0.5
3	2π	0.3

Table 3.1 Parameter sets for theoretical impulse response waveforms.

In the previous section, the length N of the vector of calculated coefficients for each Daubechies scaling function is known. This information must be identified in the case of an impulse response waveform to ensure the ability of the coefficients to capture the characteristics of the waveform. The ability of the calculated coefficients to capture the characteristics of the waveform is determined by using the coefficients in a single iteration of (3.1) with a half scale of the original waveform. This representation is called the calculated function and is then compared to the original waveform using a L^1 norm. The sufficient length N of the vector of calculated coefficients is selected when the L^1 norm error between two function is below a selected threshold error value.

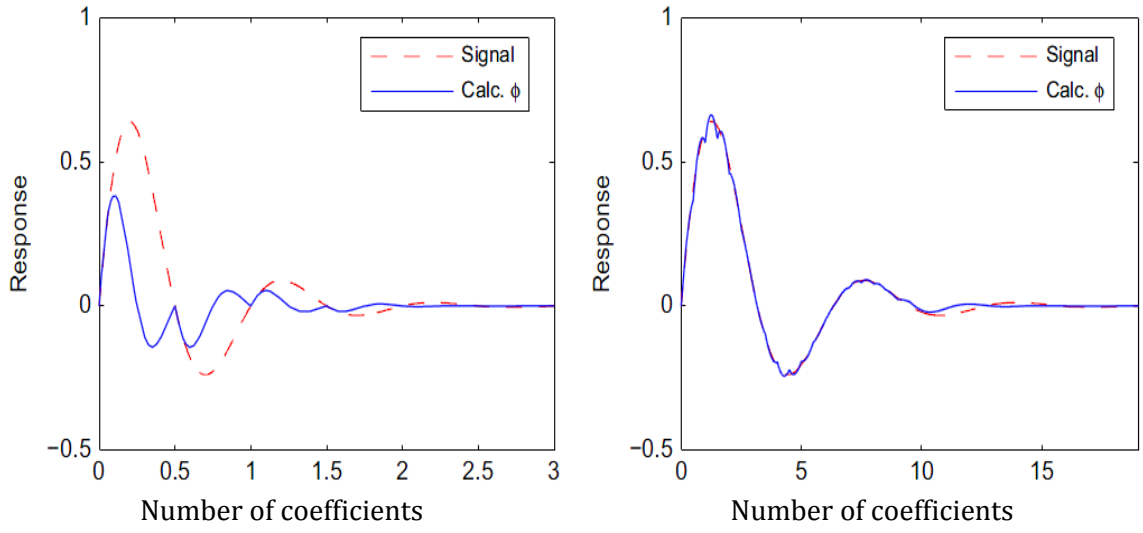

(A) (B)

Figure 3.3 Comparison of the calculated function derived by using the calculated coefficients and its half scale function to the original impulse response waveform for parameter set 1 (A) N=4 and (B) N=20.

In Figure 3.3(A), the length N of the coefficients is equal to four. The calculated function from this coefficient set clearly exhibits poor correlation with the original waveform. With an insufficient number of coefficients, the characteristics of the original waveform are not successfully captured. In Figure 3.3(B), the length N of coefficients is increased to twenty. The agreement between the calculated function and the original waveform is greatly improved. To provide a quantitative measure of the correlation, the absolute value of the difference between the calculated function and the original waveform is calculated for each length N of the calculated coefficients. The resulting error vector is numerically integrated over the non-dimensionalized time and is used to characterize the relative effectiveness of the coefficients in capturing the characteristics of the original signal for each length *N*.

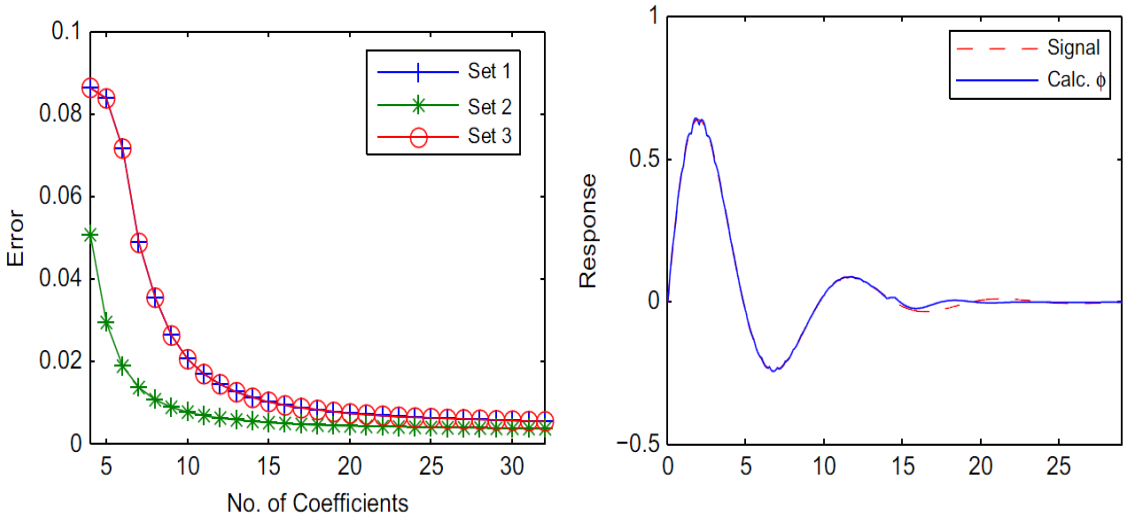

(A) (B)

Figure 3.4 (A) Plot of the error between calculated function and original waveform versus the length N of coefficients. (B) Comparison of the calculated function and the original waveform for N=30.

This error vector is used to evaluate the performance of the Formula in a range of different values of N for a particular waveform. An error function corresponding to values of $N = 4$ to $N = 20$ are plotted in (A). The magnitude of the error is much greater for $N = 4$ than for $N = 20$, reflecting the lesser ability of the shorter coefficient lengths to capture the characteristics of the waveform when compared with the longer coefficients lengths. As a result, the magnitude of the error for parameter set 1 in (A) decreases as the length of coefficients is increased. By increasing the value of N beyond 20, the error function is decreased further at a much lower rate. By increasing the number of coefficients from $N = 4$ to $N = 20$, the value of the error function decreasing by 91 percent.

When the number of coefficients is increased from *N=20* to *N=30*, the error is decreased by only 2 percents. Better agreement is observed during the first period of oscillation as seen in (B) with Figure 3.3(B). However, a deviation between two functions is observed in the second half of the scaling function in (B). The coefficient length *N=19* is sufficient to represent this waveform. The procedure uses to study the performance of the Formula with impulse response waveforms is in Figure 3.5.

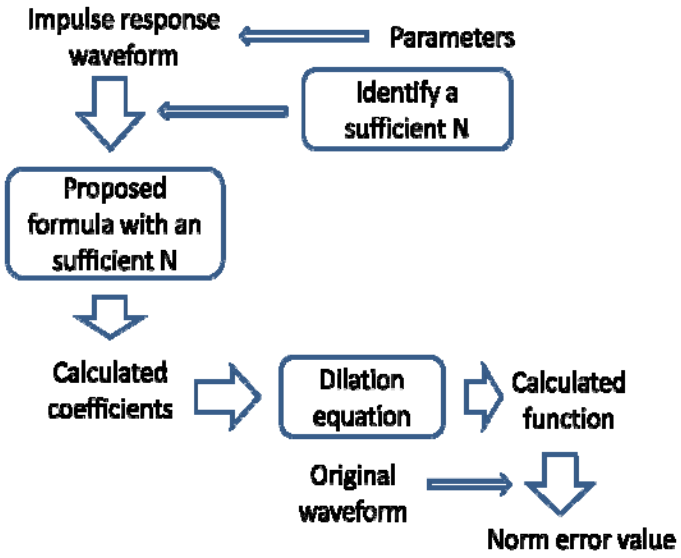

Figure 3.5 The procedure uses to convey the performance of the Formula with impulse response waveforms.

Similar assessments are repeated for waveforms that are generated by using (3.8) with the values from parameter sets two and three. The magnitude of the error for these parameter sets are also plotted in (A). A similar trend as the first parameter set is observed.

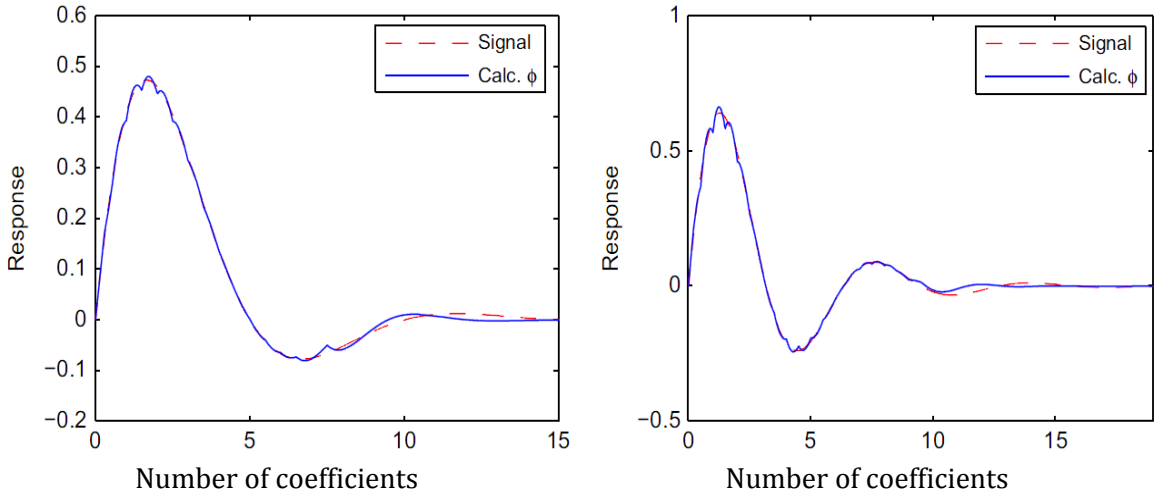

Figure 3.6 Calculated functions compared with impulse response waveforms for (A) N=16 with parameter set 2 and (B) N = 19 with parameter set 3.

Considering a threshold error value at 5 percents of the error value at *N=4*, it is observed in Figure 3.6(A) a sufficient length *N* of coefficients for parameter sets two and three are *N=16* and *N=19*, respectively. Using these values, good agreement with the impulse response waveform and the calculated function is illustrated in Figure 3.6(A) and (B) for both parameter sets. It is clear that in order to successfully capture the characteristics of a particular waveform, the length of coefficients *N* must be selected appropriately. By conducting additional simulations, it is observed that when the system damping ratio is increased, fewer coefficients are need to reproduce the original waveform. For parameter set one and parameter set three, the overlap of the error functions is observed. This behavior can be expected since the length of the signal is adjusted based on the natural frequency of the system of being studied and damping for both parameter sets are the same.

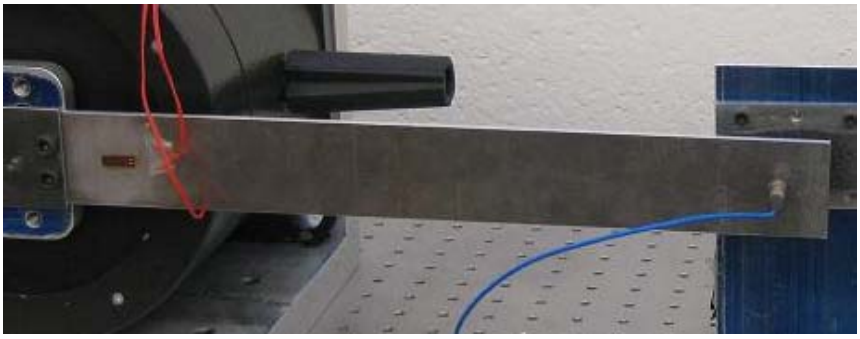

Figure 3.7 The experiment system uses a cantilevered aluminum beam with a single accelerometer to measure the resulting impulse responses.

3.3.2. Experimental waveform

From the analytical results, the performance of the Formula is depended significantly on the length of coefficients *N* and the complexity of the waveform. This section presents a study of the formula performance with an experimental impulse response waveform.

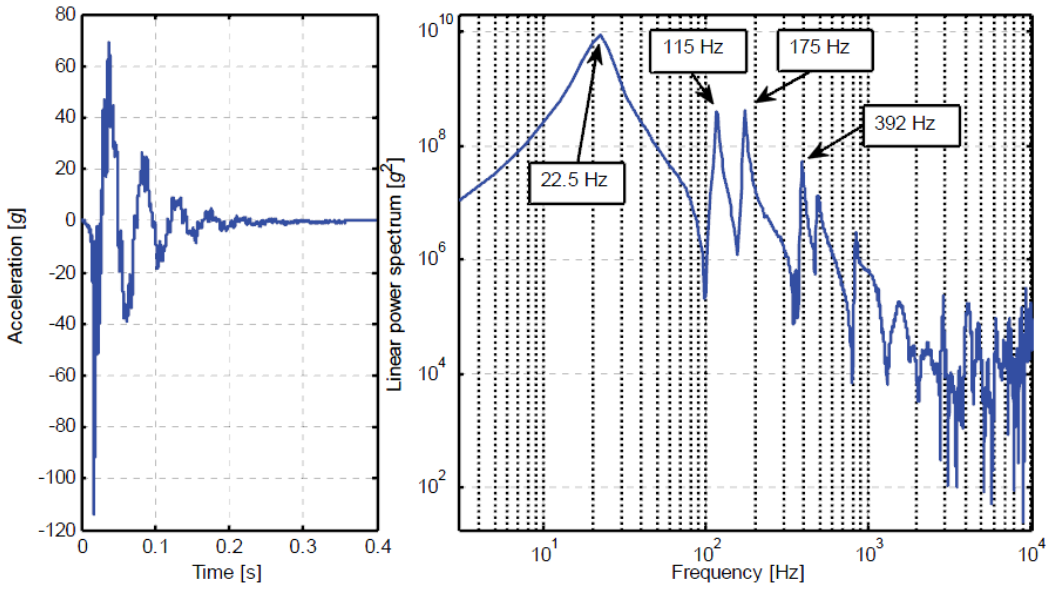

Figure 3.8 (A) The experimental acceleration waveform and (B) Autopower spectrum of the experimental waveform.

The experiment system is the cantilevered aluminum beam in Figure 3.7. The electromagnetic shaker is inactive. The geometry of the beam is 360 mm x 45 mm x 4.05 mm. The cantilever is instrumented with a PCB Piezotronics accelerometer with a sensitivity of 103.6 mV/g. The response data is collected by using a National Instruments Compact DAQ data acquisition system. The length of data record is ten seconds at a sampling rate of 50 kSa/s. The cantilevered beam is struck by impact excitations and the responses are then recorded by the National Instruments Compact DAQ data acquisition system. An impact response is shown in Figure 3.8(A). The autopower spectrum of the response is presented in Figure 3.8(B).

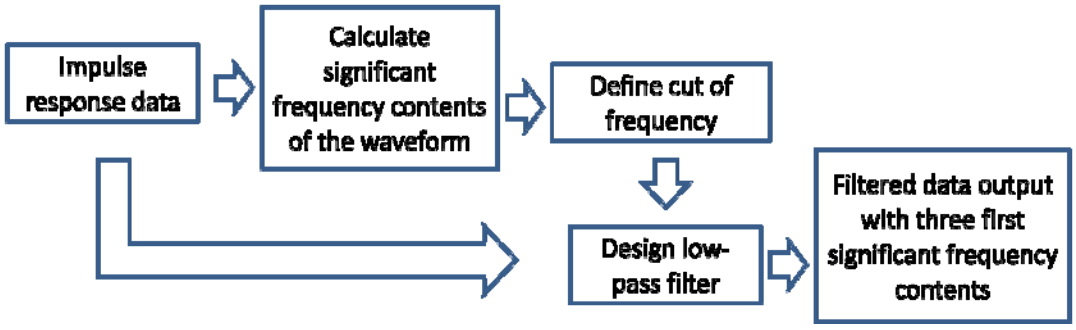

Figure 3.9 Filtering experimental waveform scheme

Significant frequency contents of the beam are indicated as peaks in the autopower spectrum. Four significant frequency components of the experimental waveform are identified in Figure 3.8(B) at 22.5 Hz, 115 Hz, 175 Hz, and 392 Hz. In order to reduce the complexity of the waveform, a filtering step is implemented by applying a low pass filter. Only the three lowest significant frequency components are kept and the high frequency contents of the waveform are removed. The cut-off frequency of the low pass filter is set to 125 Hz.

The filtering process is illustrated in Figure 3.9. A subset of 20,001 data points of the filtered signal is used as an input waveform. The same process for the analytical waveforms is implemented for the experimental waveform. An error function is generated for a range of N values from 4 to 90 and is plotted in Figure 3.10 (A).

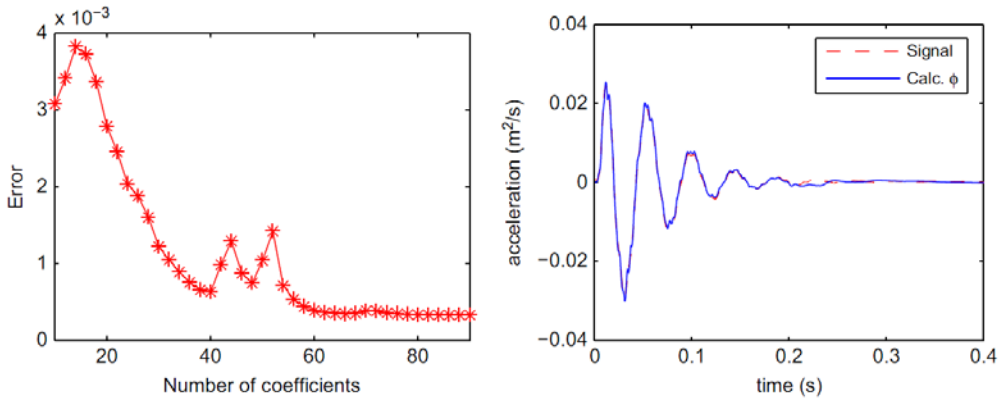

(A) (B)

Figure 3.10 (A) Plot of error between the calculated function and the experimental waveform versus the number of coefficients (B) Graphical comparison of the calculated function and the original waveform for N=60.

The result of this study is also in agreement with the previous section. For the analytical impulse response waveform, only one significant frequency component is presented. Then, at a particular length of coefficients, the error function slowly decreases after that frequency component is captured. For the experimental case, the situation is more complicated because the filtered experimental waveform has three significant frequency components. Those frequency components must be represented effectively by the calculated coefficients in order to improve agreement between the signal and the calculated function. From the error plot, there are two local minimum errors observed on the error curve. The first local minimum occurs at N=40, where the lowest frequency content

of the waveform is successfully captured. The higher error values after this value of N can be understood as an unsuccessful capture the next higher significant frequency component of the waveform. The same phenomenon is observed for the second local minimum error that appears in the error function. When the length of coefficients is increased to N=60, the three frequency components of the waveform are successfully captured. The analysis is confirmed by an agreement between the calculated waveform and the experimental waveform in Figure 3.10(B).

An evaluation the performance of the Formula with an experimental waveform confirms that the calculated coefficients can capture the characteristics of a waveform. For a more complicated waveform, the length of the coefficient set needs to increase accordingly to make sure characteristics of the waveform are captured. Analysis of the experimental waveform revealed some new characteristics of the error function. This behavior can be explained as a transition period of the error function to successfully capture the next significant frequency component of the waveform. Up to this point, the study of the performance of the Formula on Daubechies scaling functions, analytical form of the impulse response and a simplified experimental waveform confirms the ability of the Formula to calculate coefficients to capture characteristics of a waveform with a corresponding length N of coefficients.

The calculated coefficient set is then used as an input to design a new bi-orthogonal wavelet family. The characteristics of the waveform being studied are projected into primal scaling function of the new bi-orthogonal wavelet. The wavelet design process is presented in the next section.

3.4. Bi-orthogonal wavelet design process

In this section, a bi-orthogonal wavelet design process is presented. The calculated coefficients from the proposed Formula are used as an input of the process. For an impulse response waveform, the calculated coefficients are not true scaling function coefficients. A conditioned process is applied to the calculated coefficients to ensure that they satisfy the scaling function coefficient requirements in (2.10) and (2.11). The calculated coefficients are convoluted with any scaling function coefficient set. This process returns a set of coefficients that not only satisfies the scaling function coefficients condition but also guarantees for a good retention of the original waveform characteristics. On another hand, the coefficient output in general cannot form an orthogonal translation base. Therefore, the coefficients are used as primal scaling function coefficients for a new bi-orthogonal wavelet family.

From the chapter 2, the primal scaling coefficients and the dual scaling coefficients of a bi-orthogonal wavelet must satisfy constraints in (2.48). For the calculation in this illustration, ten vanishing moments are added into the dual scaling coefficients. Then, the primal wavelet coefficients and the dual wavelet coefficients are calculated by (2.42).

Nineteen coefficients that have the characteristics of an analytical impulse response for parameter set one is used for a bi-orthogonal wavelet design process. The calculated coefficient set is first refined by the DB1 scaling function coefficients to satisfy scaling function coefficient conditions. Then, the output coefficients are

normalized to have its coefficient summation is equal to two. After this process, the output coefficients are used as a primal scaling function coefficient of a new bi-orthogonal wavelet family. The primal scaling function coefficients have twenty coefficients and one vanishing moment. Values of the primal scaling function coefficients are in Table 3-column 1.

Next, the dual scaling function coefficients are designed to have the length N of coefficients equal to 20. Then, for an easy manipulation, the z transform of the dual scaling function coefficients is in (3.9).

$$\tilde{H}_0(z) = \sum_{n=0}^{19} \tilde{h}_0(n) z^{-n}. \tag{3.9}$$

Then, ten vanishing moments are added into the dual scaling function coefficients. The z transform of the dual scaling function coefficients is rearranged in (3.10) (G. Strang, T. Nguyen, 1996)

$$\tilde{H}_0(z) = (1+z^{-1})^{10} Q(z) = (1+z^{-1})^{10} (\sum_{i=0}^{9} a_i z^{-i}), \tag{3.10}$$

where a_i are the unknown coefficient i^{th} in the polynomial order of nine. The order of polynomial $Q(z)$ is nine to assure the length N of the dual scaling function coefficients is equal to twenty in the (3.10). The unknown coefficients $\tilde{h}_0(n)$ can be represented by the ten unknown coefficients a_i of the polynomial $Q(z)$ by matching the order of the polynomial $\tilde{H}_0(z)$ in (3.9) and (3.10). In addition, ten linear algebraic equations are set up by using orthogonal relationship between the

primal scaling coefficients and dual scaling coefficients in (2.48). A system of linear algebraic equations with ten unknowns and ten equations is derived. By a simple inverse process, a unique solution for the ten unknown a_i is determined. The calculated a_i values are in Table 3.2.

a(0)	*a(1)*	*a(2)*	*a(3)*	*a(4)*
0.19105777	-0.901719	2.05637	-2.9276	2.83618
a(5)	*a(6)*	*a(7)*	*a(8)*	*a(9)*
-1.92144	0.903566	-0.282671	0.0531142	-0.00454832

Table 3.2 The calculated values a(i) for calculating dual scaling function coefficients

Then, substitute the calculated a_i values into (3.10) and matching the order of the polynomial $\tilde{H}_0(z)$ in (3.9) and (3.10), the dual scaling function coefficients are determined. The values of the calculated dual scaling function coefficients are in Table 3.3 – column 2.

After having the primal and dual scaling function coefficients, the primal wavelet and its dual wavelet coefficients are ready to be calculated by using (2.42). The coefficient values of the new bi-orthogonal wavelet are listed in Table 3.3. The design process for a new bi-orthogonal wavelet family from an impulse response waveform is summarized in a diagram in Figure 3.11. As a result of the design process, the characteristics of the original waveform are projected on the scaling function coefficients and are illustrated visually in Figure 3.12. The frequency representation of the new bi-orthogonal wavelet coefficients are in Figure 3.13.

Figure 3.11 Algorithm for deriving a bi-orthogonal wavelet that has the characteristics of an impulse response waveform.

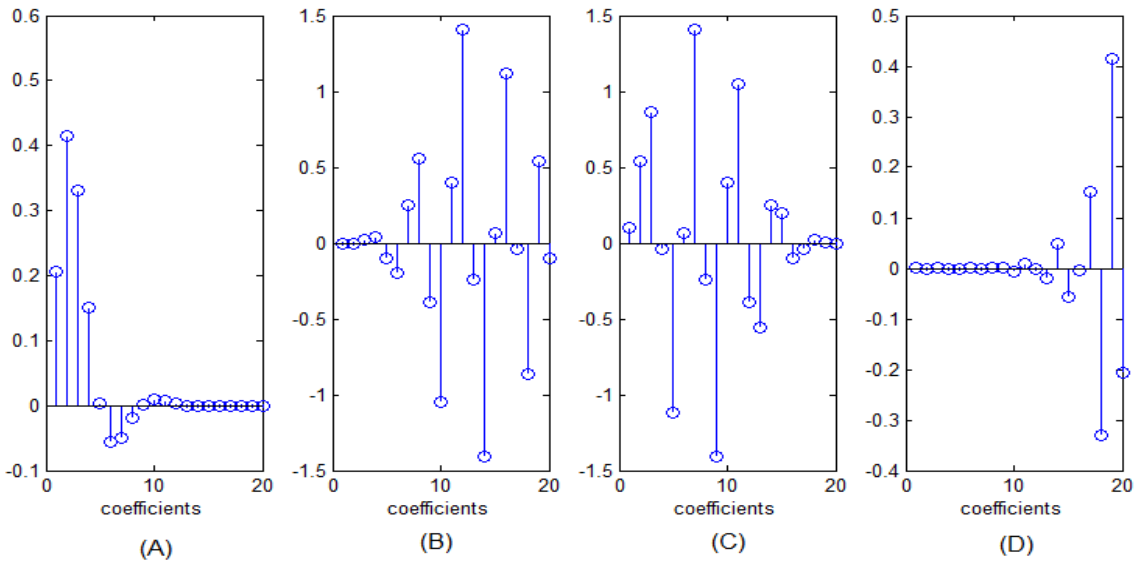

Figure 3.12 Derived bi-orthogonal wavelet coefficients (A) scaling function coefficients, (B) wavelet coefficients, (C) dual scaling function coefficients, (D) dual wavelet coefficients.

Decomposition		Reconstruction	
Primal scaling function	**Primal wavelet coefficients**	**Dual scaling function**	**Dual wavelet coefficients**
0.206455535	0.101761926	-0.002428655	0.0000414
0.415103795	0.536130613	-0.004074706	-0.000154011
0.331402298	0.862434954	0.023385961	0.000254091
0.151157899	-0.03845367	0.042078455	-0.000165385
0.003387156	-1.115073672	-0.10007523	-0.000289481
-0.056832022	0.067906784	-0.197319876	0.001061371
-0.049292387	1.404840753	0.248850859	-0.001578689
-0.019944136	-0.241738305	0.555528264	0.000722731
0.002203613	-1.407506746	-0.391968142	0.00248558
0.009601611	0.398389785	-1.049754922	-0.00730849
0.00730849	1.049754922	0.398389785	0.009601611
0.00248558	-0.391968142	1.407506746	-0.002203613
-0.000722731	-0.555528264	-0.241738305	-0.019944136
-0.001578689	0.248850859	-1.404840753	0.049292387
-0.001061371	0.197319876	0.067906784	-0.056832022
-0.000289481	-0.10007523	1.115073672	-0.003387156
0.000165385	-0.042078455	-0.03845367	0.151157899
0.000254091	0.023385961	-0.862434954	-0.331402298
0.000154011	0.004074706	0.536130613	0.415103795
0.0000414	-0.002428655	-0.101761926	-0.206455535

Table 3.3 Impulse response bi-orthogonal wavelet coefficients

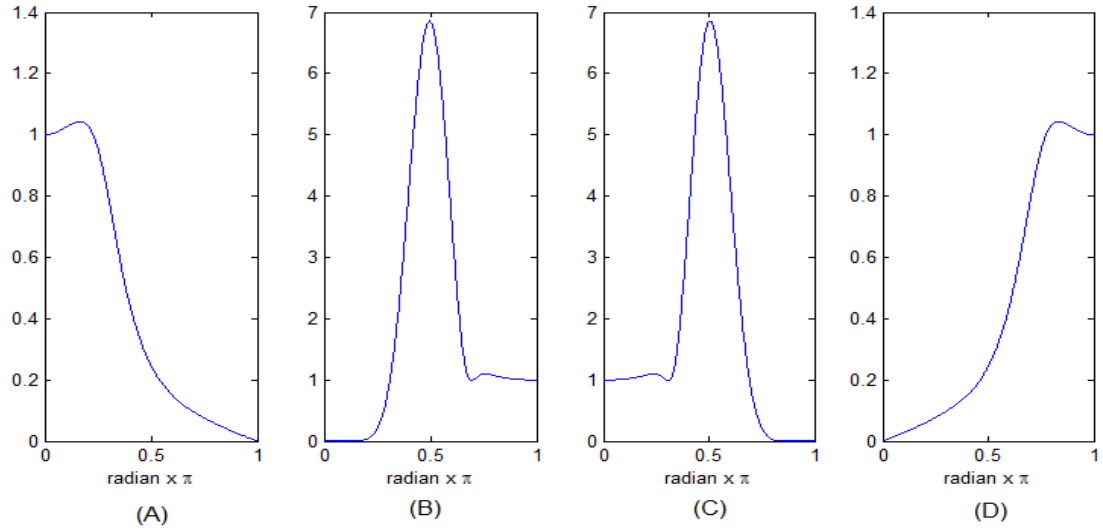

Figure 3.13 Frequency representation of the bi-orthogonal wavelet coefficients. (A) scaling function coefficients, (B) wavelet coefficients, (C) dual scaling function coefficients, (D) dual wavelet coefficients.

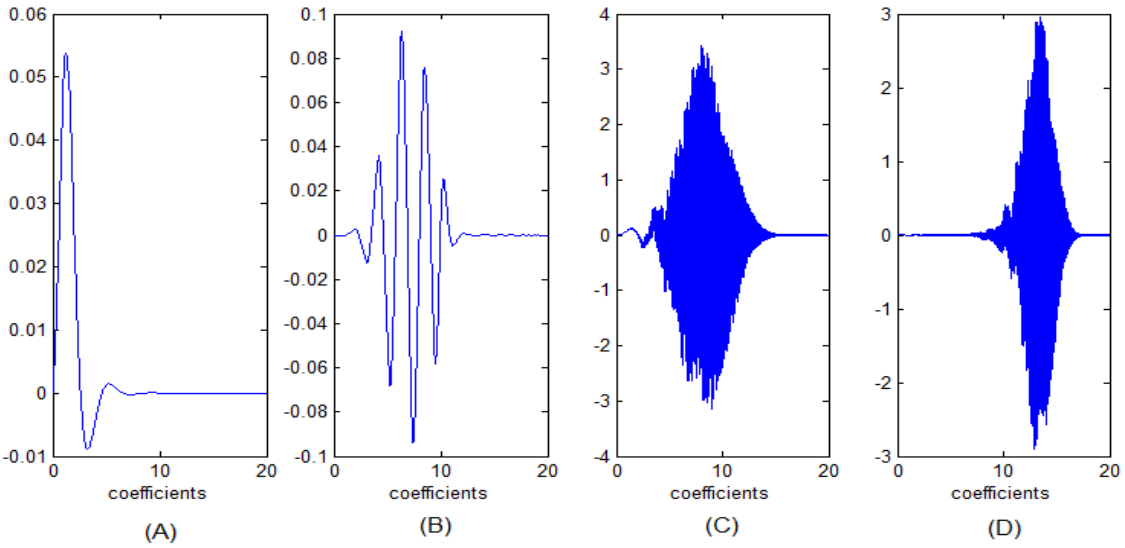

Figure 3.14 (A) primal scaling function, (B) primal wavelet function, (C) dual scaling function, (D) dual wavelet function.

A similar design process can be implemented with a desire number of vanishing moments in the new bi-orthogonal wavelet. If the number of equations in (3.13) are larger than the number of unknowns, a pseudo inverse process must be

implemented to solve for the dual scaling function coefficients. In Figure 3.14 (C) and (D), the dual scaling function and the dual wavelet function show strange behaviors although the scaling function coefficients satisfy the necessary conditions for the scaling function coefficients. The reason for the behaviors is due to the arbitrary characteristics of the calculated coefficients. The generated dual scaling function and the dual wavelet function do not convergence to one dual scaling function and dual wavelet function in this case.

3.5. New bi-orthogonal wavelet evaluation

In this section, a simple example is presented to demonstrate the ability of the new bi-orthogonal wavelet family and compare to the widely used Daubechies wavelets in the sense to enhance specific features of a signal. The generated signal is a series of four original analytical impulse responses shown in Figure 3.15, Figure 3.16 and Figure 3.17. The analytical impulse responses are the same as the original waveform that is used to calculate the scaling function coefficients of the new bi-orthogonal wavelet. In addition, a signal to noise ratio (SNR) 10dB is added to the signal to study the performance of the new bi-orthogonal wavelet with noise. It's expected that the new bi-orthogonal wavelet family provides a highest coefficient magnitude at a corresponding scale and a translation on the wavelet scalogram.

The signal is then decomposed by using the Daubechies 8 (DB8) wavelet, the Daubechies 2 (DB2) wavelet and the new bi-orthogonal wavelet. For this evaluation, the DB8 wavelet is selected because its coefficient length is closed to the

length of the new bi-orthogonal wavelet coefficients and the DB2 wavelet is selected because its coefficients have a number of vanishing moments is comparable to the new bi-orthogonal wavelet scaling function coefficients. The scalogram of the wavelet coefficients at different scales are plotted in Figure 3.15 for the new bi-orthogonal wavelet case and in Figure 3.16 for the DB8 wavelet case and in Figure 3.17 for the DB2 wavelet case. From the discrete wavelet scalogram plots, each coefficient value reflects the similarity between the wavelet at scale *a* and translation *k* and the signal of being study. The wavelet scalogram shows equally high amplitude coefficients at scale 9 for the bi-orthogonal wavelet case and at scale 10 for the DB8 wavelet case. The coefficients at the previous and next scales in the wavelet scalogram for the Daubechies wavelet case shows a smaller amplitude than it's of the new bi-orthogonal wavelet case. Therefore, the new bi-orthogonal wavelet does not outperform the Daubechies wavelet in localizing characteristics of the waveform in this evaluation. This is cause by the wavelet of the new bi-orthogonal wavelet being in a different form from the signal of being study although the primal scaling function coefficients sharing characteristics with the signal being studied. The new bi-orthogonal wavelet coefficients which plotted in confirm this observation. However, the dispersion effect of the wavelet coefficients in the wavelet scalogram of the new bi-orthogonal wavelet is better than that of the wavelet scalogram of the DB2 wavelet. The scalograms confirm that three wavelets successfully remove noise effects at high scales. The study suggests that the number of vanishing moments in the wavelet contributes to this behavior of the wavelet coefficient value.

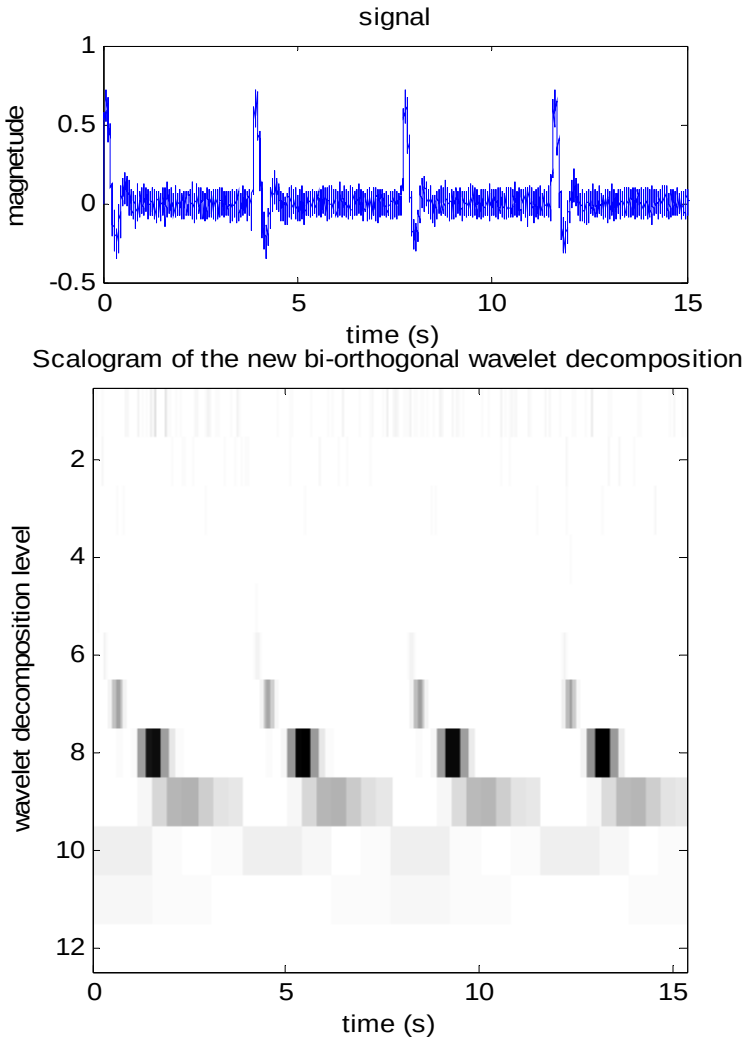

Figure 3.15 Discrete wavelet scalogram using the new bi-orthogonal wavelet

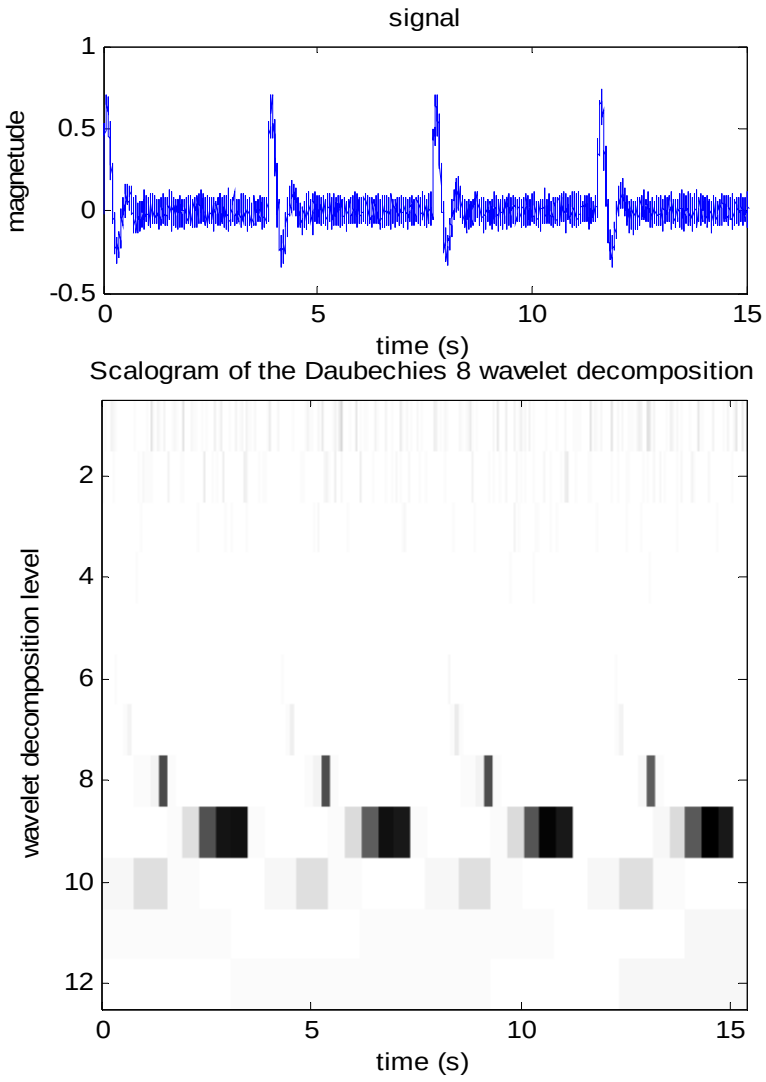

Figure 3.16 Discrete wavelet scalogram using the Daubechies 8 wavelet

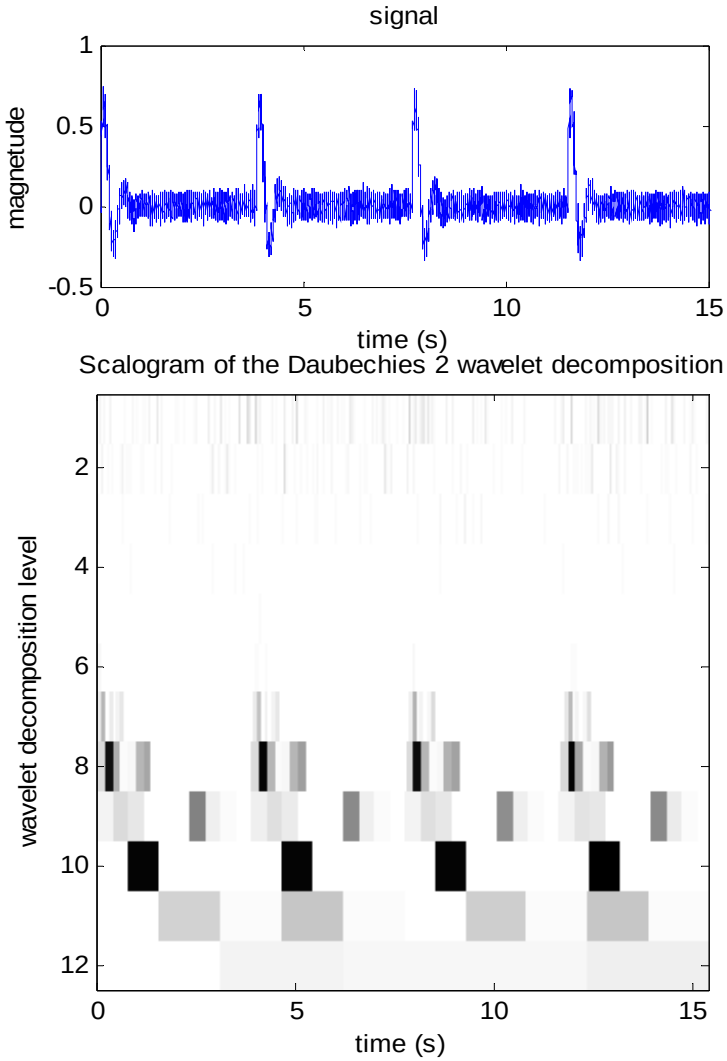

Figure 3.17 Discrete wavelet scalogram using the DB 2 wavelet

3.6. Summary

By using the dilation equation, a Formula is derived for calculating a coefficient vector from a given discrete waveform. The Formula is first applied to waveforms that correspond to the approximated Daubechies scaling functions. Excellent agreements between the calculated coefficients and true values of the Daubechies coefficients are observed. In addition, for a better approximation of the waveform to the true Daubechies scaling function, the absolute error between the calculated coefficients and the true values of the Daubechies coefficients is reduced. Next, the performance of the Formula is studied by using impulse response waveforms of analytical models and an experimental system. A qualitative criterion is developed to identify a sufficient length N of coefficients to capture characteristics of a input waveform. It is also showed that a sufficient length N of coefficients is related to the complexity of the input waveform. Later, a process is required for the calculated coefficients to satisfy the strict conditions of the scaling function coefficients. The output coefficients of the process are used as primal scaling function coefficients of a new bi-orthogonal wavelet. Then, the performance of the new bi-orthogonal wavelet is evaluated by comparing it to the widely used Daubechies wavelet family in analyzing a signal that has similar characteristics to the original waveform. The result of the evaluation process shows that the new bi-orthogonal wavelet provides comparable performance to the popular Daubechies wavelet with a similar number of vanishing moments in this evaluation process.

Chapter 4

Concluding remarks and future work

The wavelet transform provides a variety of options for researchers to study time varying signals. In this thesis, the aim was to develop a new wavelet derived directly from the signal being studied. By using the dilation equation, a Formula was derived for calculating a coefficient vector for a given discrete waveform. Then, a bi-orthogonal wavelet family was derived directly from the calculated coefficients. The evaluation process for the new bi-orthogonal wavelet with a waveform that has the same characteristics to the original waveform was performed. The study showed that the new bi-orthogonal wavelet provided a better performance than DB2 wavelet in this evaluation. When compared to the Daubechies 8, the Daubechies wavelet provided better performance in localizing characteristics of the signal than the new bi-orthogonal wavelet. It is suggested that a further study

should be performed to identify the strengths of the new bi-orthogonal wavelet family.

In conclusion, the thesis work studies the performance of the proposed Formula to calculate coefficients to represent an impulse response waveform by its half scale waveform. A new bi-orthogonal wavelet family was designed and provided a new wavelet option for signal processing applications.

References

A. Cohen, I. D. a. J. C. F., 1992. Bi-orthogonal bases of compactly supported wavelets. Volume 45, pp. 485-560.

A. Gupta, S. J. S. P., 2005. A new method to estimating wavelet with desired features from a given signal. 85(1), pp. 147-161.

A.H. Tewfix, D. S. P. J., 1992. On the optimal choice of a wavelet for signal representation. 38(2), pp. 747-765.

A.J. Dick, Q. P. J. F. P. S., 2012. Calculating scaling function coefficients from system response data for new discrete wavelet families. Volume 27, pp. 362-369.

B. Zeldin, P. S., 1996. Random field representation and synthesis using wavelet bases. Volume 63.

Bussow, R., 2008. Bending wavelet for flexural impulse response. 123(4), pp. 2126-2135.

C. Juncheng, Y. D. Y. Y., 2007. Application of an impulse response wavelet to fault diagnosis of rolling bearing. Volume 21, pp. 920-929.

C.K.Chui, 1992. *An introduction to wavelets.* s.l.:Academic Press.

C.M. Harris, A. P., 2002. *Shock and Vibration Handbook.* New york: McGraw-Hill.

C.S. Burrus, R. G. H. G., 1997. *Introduction to wavelets and wavelet transforms: A Primer.* s.l.:Prentice Hall Press.

Cohen, L., 1989. *Time frequency distribution-a review.* s.l., s.n., pp. 941-981.

D. Boulahbal, M. G. F. I., 1999. Amplitude and phase wavelet maps for the detection of cracks in geared systems. *Mechanical system and signal processing,* 13(3), pp. 423-436.

D. Maraun, J. K., 2004. Cross wavelet analysis: significance testing and pitfalls. *Nonlinear processes in Geophysics,* Volume 11, pp. 505-514.

Daubechies, I., 1988. Orthonormal bases of compactly supported wavelets. Volume 41, pp. 909-996.

Daubechies, I., 1992. *Ten lectures on wavelets.* Philadelphia, PA: SIAM.

Dick, A., 2010. *Wavelet analysis of structural anomalies using baseline impulse response,* s.l.: AFRL .

E.L. Schukin, R. S., 2004. The optimization of wavelet transform for the impulse analysis in vibration signals. 18(6), pp. 1315-1333.

G. Strang, T. Nguyen, 1996. *Wavelets and filter banks.* s.l.:Wellesley-Cambridge Press.

J. Kovacevic, A. C., 2007. Life beyond bases: The advent of frames (part II). 24(4), pp. 115-125.

J. Kovacevic, A. C., n.d. Life beyond bases: The advent of frames (part I). 24(4), pp. 86-104.

J. Ling, L. Q., 2000. Feature extraction based on Morlet wavelet and its application for mechanical fault diagnosis. 234(1), pp. 135-148.

J. Rafiee, M. R. P. T., 2010. Application of mother wavelet functions for automatic gear and bearing fault diagnosis. Volume 34, pp. 4568-4579.

J.O. Chapa, R. R., 2000. Algorithms for designing wavelets to match a specified signal. 48(12), pp. 3395-3406.

L.E. Suarez, L. M., 2005. Generation of artificial earthquakes via the wavelet transform. 42(21-22), pp. 4905-5919.

L.K. Shark, C., 2003. Design of optimal shift-invariant ortho-normal wavelet filter banks via genetic algorithm. 83(12), pp. 2579-2591.

Mallat, S., 1989. A theory for multiresolution signal decomposition: The wavelet representation. 11(7), pp. 674-693.

Newland, D., 1993. *An introduction to random vibrations, spectral & wavelet analysis.* New york: Dover Publications.

Newland, D., 1993. *Harmonic wavelet analysis.* s.l., Proc. R. Soc. Lond. A, pp. 203-225.

Newland, D., 1994. *Harmonic and musical wavelets.* s.l., Proc. R. Soc. Lond. A., pp. 605-620.

P. Goupillaud, A. G. J. M., 1984. Cycle-Octave and related transforms in seismic signal analysis. Volume 23, pp. 85-102.

P.D. Spanos, G. F., 2005. Theoretical concepts and vibrations related applications. 37(5), pp. 359-375.

P.D. Spanos, R. L., 1995. Nonlinear system identification in offshore structural reliability. *Journal of Offshore Mechanics and Arctic Engineering,* Volume 17, pp. 171-177.

P.D. Spanos, V. R. S. R., 2001. Random field representation in a bi-orthogonal wavelet basis. 127(2).

P.S. Addison, J. W. T. F., 2002. Low-oscillation complex wavelets. 254(4), pp. 733-762.

Penrose, R., 1955. *A generalized inverse for matrices.* s.l., Proceedings of the Cambridge Philosophical Society, pp. 406-413.

R. Foley, J. D. A. D. Q. P. P. S. J. V. K. G. F., 2011. *Development of new discrete wavelet families for structural dynamic analysis.* s.l., IMAC XXIX A Conference and Exposition on Structural Dynamics.

R. Yan, R. G., 2009. Wavelet selection for bearing defect diagnosis. pp. 575-582.

R. Yan, R. G., 2010. *Design of an impulse wavelet for structural defect identification.* Macau, China, IEEE PHM.

S. Mikami, S. B. T. O., 2011. Wavelet packet based damage detection in beam like structures without baseline modal parameters. 7(3), pp. 211-227.

S. Nagarajaiah, B. B., 2009. Output only modal identification and structural damage detection using time frequency & wavelet techniques. Volume 8, pp. 583-605.

S.N. Fernando, M. R., 2006. *Application of wavelets to identify faults during impulse tests,* Kansas City, MO: s.n.

Staszewski, W., 1998. Identification of nonlinear systems using multi-scale ridges and skeletons of the wavelet transform. 214(4), pp. 639-658.

Strang, G., 1989. Wavelets and dialtion equations: A Brief Introduction. 31(4), pp. 614-627.

Walter, G., 1994. *Wavelets and other orthogonal systems with applications.* s.l.:CRC Press.

Weaver, H., 1993. *Applications of discrete and continuous Fourier analysis.* s.l.:John Wiley & Sons.

X. Jiang, S. M., 2011. Wavelet spectrum analysis approach to model validation of dynamic systems. Volume 25, pp. 575-590.

Z. Kunpeng, W. S. H. S., 2009. Wavelet analysis of sensor signals for tool condition monitoring: A review and some new results. Volume 49, pp. 537-553.

Z.K. Peng, F. C., 2004. Application of the wavelet transform in machine condition monitoring and fault diagnostics: A review with biliography. Volume 18, pp. 199-221.

Appendix I: The Moore Penrose inverse procedure

The Moore Penrose inverse procedure is used to calculate the inverse of non-square *mxn* matrix B. Call B^H is the conjugate transpose of matrix B. Then, the inverse of the matrix B can be calculated by (A1.1):

$$B^+ = (B^H B)^{-1} B^H \qquad (A1.1)$$

If the matrix $(B^H B)$ is singular, the procedure has more than one solution. Then, Matlab provides two solutions to calculate the inverse of the matrix B by using *backslash* operator and *pinv* function. For the first case, the backslash operator provides a basic solution. The *pinv* function provides a minimum norm error solution. In this thesis, the backslash operator is used to calculate inverse of a non-square matrix.